

C.1

Copy 5
RM L54G12a

NACA RM L54G12a

*Whitcomb
atg*



RESEARCH MEMORANDUM

FOR REFERENCE

NOT TO BE TAKEN FROM THIS ROOM

EFFECTS OF OVERHANG BALANCE ON THE HINGE-MOMENT AND
EFFECTIVENESS CHARACTERISTICS OF AN UNSWEPT
TRAILING-EDGE CONTROL ON A 60° DELTA WING
AT TRANSONIC AND SUPERSONIC SPEEDS

By Lawrence D. Guy

Langley Aeronautical Laboratory
Langley Field, Va.

CLASSIFICATION

UNCLASSIFIED

RESEARCH REPORT

SEP 15 1954

To: _____
By authority of *NACA Res abs Effective
+ RN-129* Date *July 17, 1958*

CLASSIFIED DOCUMENT

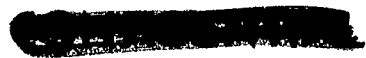
Int 10-2-58

This material contains information affecting the National Defense of the United States within the meaning of the espionage laws, Title 18, U.S.C., Secs. 793 and 794, the transmission or revelation of which in any manner to an unauthorized person is prohibited by law.

NATIONAL ADVISORY COMMITTEE FOR AERONAUTICS

WASHINGTON

September 14, 1954



NATIONAL ADVISORY COMMITTEE FOR AERONAUTICS

RESEARCH MEMORANDUM

EFFECTS OF OVERHANG BALANCE ON THE HINGE-MOMENT AND
EFFECTIVENESS CHARACTERISTICS OF AN UNSWEPT
TRAILING-EDGE CONTROL ON A 60° DELTA WING
AT TRANSONIC AND SUPERSONIC SPEEDS

By Lawrence D. Guy

SUMMARY

An investigation of a 60° delta wing equipped with an unbalanced and with a 100-percent overhang balanced constant-chord flap-type control was conducted in the Langley 9- by 12-inch blowdown tunnel. Control hinge moments and aerodynamic characteristics of the complete semispan-wing-body combination were obtained over an angle-of-attack range of $\pm 12^\circ$ for control deflections up to 40° . Data were obtained at Mach numbers from 0.75 to 1.25 and at Mach numbers of 1.41, 1.62, and 1.96.

At all Mach numbers the unbalanced control was effective for all conditions of control deflection and angle of attack, and hinge moments varied in a nearly linear manner with control deflection and with angle of attack. The large hinge moments were considerably reduced by moving the hinge line to the midchord point but at the expense of control effectiveness. The balancing action of the resulting overhang area, however, was not uniform and hinge moments varied with control deflection in a highly nonlinear fashion. In general, the result was an overbalanced condition at subsonic speeds and an underbalanced condition at supersonic speeds. The balancing effects at subsonic speeds were greatest before the control unported and at supersonic speeds greatest after the control unported.

With the control deflected to produce a given roll rate, the magnitudes of the hinge moments were much smaller for the balanced control and showed less change with Mach number than for the unbalanced control. Comparison on the basis of deflection work for the same roll rate, however, showed somewhat less advantage to the balanced control at moderate angles of attack for supersonic speeds.

Comparison of control characteristics with data obtained in other facilities presents strong justification for the technique of testing shinned semispan-wing-control models of practical size in the transonic slotted nozzle.

INTRODUCTION

The very large hinge moments developed by trailing-edge flap-type controls at transonic and supersonic speeds have encouraged research on various means of balancing such controls aerodynamically. Controls having nose overhang balance areas have been used successfully to reduce these large hinge moments at high subsonic speeds. The hinge-moment variations, however, are found to be very nonlinear and the controls have sizable changes in balance characteristics with Mach number in the transonic speed range (refs. 1 to 4). At supersonic speeds, substantial reductions in aerodynamic balance occur and greater amounts of nose overhang are required for balancing than at subsonic speeds (refs. 2 and 5). It is desirable to obtain further information on this type of aerodynamic balance at both transonic and supersonic speeds. In order to furnish such information, investigations of 60° delta wing models having similar wing geometry and constant-chord trailing-edge flaps have been made in the Langley 7- by 10-foot tunnel transonic-bump method and in the Langley 9- by 12-inch blowdown tunnel. The transonic-bump investigation of the model, which had varying amounts of control balance, was made at Mach numbers of 0.60 to 1.18 and is reported in reference 6. The investigation, reported herein, of the hinge-moment and effectiveness characteristics of the model tested in the blowdown tunnel has been made for two control hinge-line locations at Mach numbers from 0.75 to 1.96.

The model was tested with each control throughout an angle-of-attack range of $\pm 12^\circ$ and a control-deflection range from 0° to 40° . One control was unbalanced except for the nose radius and the other had a hinge line set back to 50 percent of the control chord from the control nose. A new transonic nozzle, having generally satisfactory tunnel-clear flow properties was used to obtain control characteristics at Mach numbers of 0.75 to 1.25. The effects of boundary interference on model data, however, were unknown for this nozzle. Lacking definite information, comparison with related data from other facilities has been emphasized.

Theoretical expressions are derived in an appendix for the hinge-moment coefficient due to angle of attack of constant-chord, partial-span control surfaces on triangular wings for the case where the flap span does not extend to either the wing tip or the wing center line. The derivations and formulas are restricted to the case where the Mach line from the wing apex is ahead of the wing leading edge and are subject to all limitations of linear theory.

SYMBOLS

C_L	lift coefficient, $\frac{\text{Lift}}{qS}$
C_D	drag coefficient, $\frac{\text{Drag}}{qS}$
C_m	pitching-moment coefficient (pitching-moment reference axis located at $0.25\bar{c}$), $\frac{\text{Pitching moment}}{qS\bar{c}}$
$C_{l_{\text{gross}}}$	gross rolling-moment coefficient (rolling-moment reference axis shown in fig. 1), $\frac{\text{Semispan-model rolling moment}}{2qSb}$
C_h	control hinge-moment coefficient, $\frac{\text{Hinge moment}}{qb_f\bar{c}_f^2}$
$C_l, \Delta C_L, \Delta C_m$	increment in gross rolling-moment coefficient, lift coefficient, and pitching-moment coefficient, respectively, due to deflection of control surface
q	free-stream dynamic pressure
S	semispan wing area (including area blanketed by half body of revolution)
S'	area of triangular region of integration
c	local wing chord
c_r	wing root chord
\bar{c}	mean aerodynamic chord of wing
c_b	chord of control balance ahead of hinge line
c_f	control chord back of hinge line
\bar{c}_f	mean aerodynamic chord of portion of control behind hinge line
c_t	total control chord less nose radius

b	wing span, twice distance from rolling-moment reference axis to wing tip
b_f	control surface span
α	angle of attack measured with respect to free stream
δ	control-surface deflection measured perpendicular to hinge line from wing-chord plane
R	Reynolds number based on mean aerodynamic chord of wing
M	Mach number
ΔM	maximum deviation from average test section Mach number

$$m = \frac{\tan \epsilon}{\tan \mu}$$

w	deflection work, $b_f \bar{c}_f^2 \left[\int_0^{\delta} c_h d\left(\frac{\delta}{57.3}\right) + \int_0^{-\delta} c_h d\left(\frac{\delta}{57.3}\right) \right]$
---	--

μ Mach angle

P local pressure difference between lower and upper surface of airfoil, positive in sense of lift

ϕ control trailing-edge angle

Subscripts:

α slope of curve of coefficient plotted against α : $\partial c_h / \partial \alpha$, $\partial C_L / \partial \alpha$, and so forth

δ slope of curve of coefficient plotted against δ : $\partial c_l / \partial \delta$, $\partial C_h / \partial \delta$, and so forth

DESCRIPTION OF MODEL

The principal dimensions of the semispan-wing-body combination are given in figure 1 and a photograph of the model is shown in figure 2. The wing had a delta plan form with 60° leading-edge sweepback and a corresponding aspect ratio of 2.3. A constant-chord, partial-span control surface was located at the wing trailing edge such that the control inboard end was adjacent to the fuselage.

The main wing panel, exclusive of the control surface, was of solid steel and had 4-percent-thick hexagonal airfoil sections modified at the leading and trailing edge by a small radius. A body consisting of a half body of revolution together with 0.25-inch shim was integral with the main wing panel for all tests.

Two control surfaces of identical plan form and airfoil section and machined from heat-treated steel were used in the investigation. The control chord was $0.105\bar{c}$, the control span $0.535b/2$, and the control nose radius was $0.075c_f$. One control was unbalanced and had a nose overhang equal to the nose radius; the other control had a hinge line set back to 50 percent of the control chord so that it had a 100-percent overhang balance. The controls were hinged to the main wing panel by a 0.040-inch-diameter steel pin at the outboard end. At the inboard end a 0.109-inch-diameter shaft, integral with the control surface, extended through a bearing and a clamp which were part of an electrical-strain-gage beam contained within the test body. The control deflection could be changed by loosening the clamp.

TUNNEL

The tests were conducted in the Langley 9- by 12-inch blowdown tunnel which operates from the compressed air of the Langley 19-foot pressure tunnel. The absolute stagnation pressure of the air entering the test section ranges from 2 to $2\frac{1}{3}$ atmospheres. The compressed air is conditioned to insure condensation-free flow in the test section by being passed through a silica-gel drier and then through banks of finned electrical heaters. Criteria for condensation-free flow were obtained from reference 7. Turbulence damping screens are located in the settling chamber. Four interchangeable nozzle blocks provide test section Mach numbers of 0.70 to 1.25, 1.41, 1.62, and 1.96.

Supersonic Nozzles

Test section flow characteristics of the three supersonic fixed Mach number nozzles were determined from extensive calibration tests and are reported in reference 8. Deviation of flow conditions in the test section with the tunnel clear are presented in the following table:

Reynolds number (approx.)	3.0×10^6	2.6×10^6	2.4×10^6
Average Mach number	1.41	1.62	1.96
Maximum deviation in Mach number	± 0.02	± 0.01	± 0.02
Maximum deviation in stream angle, deg . .	± 0.25	± 0.20	± 0.20

████████████████████

Transonic Nozzle

The transonic nozzle has a 7- by 10-inch rectangular test section slotted on three sides and solid on the fourth (10-inch) side from which the model was mounted. The ratio of open area to closed area of the three slotted walls is 0.11. Preliminary calibration tests of the transonic nozzle have indicated satisfactory test section flow characteristics from the minimum Mach number ($M = 0.7$) to about $M = 1.20$. The maximum deviations from the average Mach number in the region occupied by the model are shown in figure 3. The Mach number was determined by static-pressure surveys made with the tunnel clear, the total head pressure being assumed equal to the stagnation pressure in the settling chamber. The ratio of the static pressure in the plenum chamber surrounding the test section to the settling-chamber pressure was used as a reference for calibration tests and for establishing Mach number and dynamic pressure during model tests. Limited stream angle surveys were made by using a pressure probe similar to the prism-type combination probe of reference 9. The stream-angle data, available only in a plane containing the tunnel center line at one tunnel longitudinal station, show that, over the region spanned by the model, the stream angle did not exceed $\pm 0.1^\circ$ at any Mach number. The test section Mach number decreased about 0.015 as the model angle of attack was changed from 0 to $\pm 12^\circ$.

The variation with Mach number of the average Reynolds number of the tests is given in figure 3 together with the approximate limits of the variation during the test series.

ACCURACY OF DATA

An estimate of the probable errors introduced in the present data by instrument-reading errors, measuring-equipment errors, and calibration errors are presented in the following table:

Variable	Error
C_L	± 0.005
C_z	± 0.0005
C_m	± 0.001
C_h , unbalanced flap	± 0.008
C_h , balanced flap	± 0.030
α , deg	± 0.05
δ , unbalanced flap, deg	± 0.15
δ , balanced flap, deg	± 0.25

████████████████████

It should be noted that the apparent differences in the hinge-moment-coefficient errors for the two flaps is a result of the differences in control dimensions on which the data were reduced. The repeatability of the data also indicated a smaller error than that given for C_h .

The indicated error in δ is the error in the no-load control setting. Corrections determined statically as a function of hinge moment have been applied to the data for the additional variation in control deflection due to control loading. For 0° , 5° , and 10° deflection of the balanced control, the accuracy of the initial control settings relative to each other were much greater than those indicated. In this control deflection range, differences in deflections were measured by means of an optical system with an error of only $\pm 0.1^\circ$.

The errors in pitching moment given represent the relative accuracy of the pitching-moment measurements (the accuracy of each data point with respect to the other data points at the same lift coefficient). The absolute accuracy of the measurements is not known, however, because, subsequent to the measurements, the balance was modified and since the modification the pitching-moment data cannot be repeated. There is a consistent unexplained discrepancy between data obtained before and after the modification which amounts to an indicated difference in aerodynamic-center location of approximately 0.05 inch (0.01c).

TEST TECHNIQUE

The model was cantilevered from a five-component strain-gage balance set flush with the tunnel floor. The model and balance rotated together as the angle of attack was changed. The aerodynamic forces and moments on the semispan-wing-body combinations were measured with respect to the body axes and then rotated to the wind axes. Control-surface hinge moments were measured by means of an electrical-strain-gage beam contained within the test body. The body consisted of a half body of revolution mounted on a 0.25-inch shim; the shim was used to minimize the tunnel-wall boundary-layer effects on the flow over the surface of the body of revolution (ref. 10). A clearance gap of 0.010 to 0.020 inch was maintained between the fuselage shim and the tunnel floor.

VALIDITY OF TRANSONIC NOZZLE DATA

No corrections are available to allow for lift interference or blockage of the tunnel boundaries or reflection-plane interference at subsonic Mach numbers. Unpublished results of tests of a semispan 6-percent-thick, 45° sweptback wing of aspect ratio 4 in this tunnel, however, have shown

good agreement with results of tests of similar wing-fuselage models of identical geometry in the Langley 8-foot and 16-foot transonic tunnels at transonic speeds. These data show that the variation with angle of attack of the lift and pitching-moment coefficients for the wing plus fuselage interference (obtained by subtraction) were in excellent agreement over the approximately linear lift range for Mach numbers of 0.7 to 1.02 (the present limit of blowdown-tunnel tests on that model) and up to lift-coefficient values of 0.9 for Mach numbers of 0.7 to 0.94. Such agreement was not expected since, for the blowdown-tunnel tests, the ratio of model wing area to tunnel cross-sectional area was 16 percent as compared with 2.33 percent for the 8-foot tunnel tests and 4.5 percent for the 16-foot tunnel tests. Models comparable in size (on the basis of the ratio of wing area to tunnel cross-sectional area) to even the 16-foot tunnel model are too small for practical use in the blowdown tunnel, at least with the present instrumentation.

Reflection by the tunnel walls of the model shock and expansion waves back on to the model may appreciably affect the variation with α of the model force and moment coefficients between $M = 1.00$ and $M = 1.25$. Loading of the wing and control due to control deflection, however, should not be greatly affected by reflected disturbances except perhaps indirectly through alteration of the boundary-layer characteristics. It should be pointed out that the effects of reflected shock and expansion waves would not be as severe in this, a rectangular tunnel, as in a circular tunnel since the reflection of a conical wave from a straight wall tends to be diffused whereas the reflection from a concentric circular wall tends to be concentrated, or focused, at the center line.

In order to aid the evaluation, at transonic speeds, of the test technique employed in this investigation and, to some extent, of the influence of tunnel boundaries on the data obtained, the control characteristics of the present model are compared with those for nearly similar models tested in other facilities (figs. 4 to 6).

The values of $C_{h\alpha}$ and $C_{h\delta}$ obtained for the control of the present model were for the most part smaller than those obtained for the models in the other facilities. (See fig. 4.) This result may be attributed largely to differences in control geometry (see table on fig. 4) in that the control of the present model did not extend to the wing tip as did the controls of most of the other models. The result of adding control area at the wing tip is shown by the stability-tunnel data for $M = 0.17$. Extending the control to the tip increased the value of $C_{h\alpha}$ by 0.0044 and the value of $C_{h\delta}$ by a lesser amount, 0.0023. If this result is considered, the data of the present tests would be in good agreement with the data obtained in the Ames 6- by 6-foot tunnel which have been corrected for tunnel-wall lift interference and blockage. It is believed that comparison with the data from the Ames 6- by 6-foot

tunnel is more valid than comparison with the data from the Ames 12-foot pressure tunnel because, although the blowdown tunnel model and the 6-foot tunnel model differ in airfoil section, the control trailing-edge angles were nearly equal.

The trends of the variation of $C_{h\alpha}$ and $C_{h\delta}$ with Mach number for the present model are supported in the transonic-speed range by the data from the rocket-propelled-model tests. Comparison of the magnitudes of the hinge-moment parameters cannot be made because of the differences in the model geometry and in the results for the two rocket models.

The model used in the transonic-bump method differed from the present model in that it was tested without a fuselage, the control inboard end was at the wing root, and the control chord was slightly larger (see fig. 5). The values of $C_{h\alpha}$ and $C_{h\delta}$ for the models equipped with unbalanced controls are in excellent agreement. Values of $C_{h\delta}$ for the models having controls with setback hinge lines also agree very well, although this agreement may be somewhat fortuitous when consideration is given to the accuracy of the hinge-moment coefficients and control-deflection measurements. Values of $C_{h\alpha}$ for this control, however, agreed only up to Mach number 0.95 and again at $M = 1.18$. Between Mach numbers of 0.95 and 1.18, values of $C_{h\alpha}$ obtained in the Langley 9- by 12-inch blowdown tunnel were considerably larger than those obtained by the transonic-bump method. The reason for this difference is not known and repeat tests including tests made with fixed transition gave the same results. Conceivably, above $M = 1.0$, the blowdown-tunnel data were affected by reflected shock waves from the sides of the tunnel. The greatest difference between the two tests, however, occurred near $M = 1.00$ and in this region the values of $C_{h\alpha}$ for the unbalanced controls were in good agreement.

In figure 6 the variation with deflection of C_L , C_m , and C_h for the 100-percent overhang balanced controls of both the blowdown-tunnel model and the transonic-bump model are compared at two angles of attack at Mach numbers of approximately 0.9 and 1.15. It should be remembered that the models are not identical and that the values of lift and pitching-moment coefficient due to angle of attack are not comparable, principally because of the absence of a fuselage on the transonic-bump model. It can be seen, however, that the trends shown by the variation of C_L , C_m , and C_h with deflection are in good agreement. The only notable exceptions occur at the lower Mach number where the break in the pitching-moment and hinge-moment curves is shown to occur at a smaller negative deflection for the blowdown-tunnel model.

From the foregoing discussion, it appears that the transonic nozzle is a reliable test facility for obtaining wing and control characteristics due to angle of attack at high subsonic speeds and for obtaining control characteristics due to control deflection throughout the Mach number range from 0.7 to 1.2 by means of shimmied semispan models of practical size (wing area equal to 20 percent tunnel cross-sectional area).

RESULTS AND DISCUSSION

The aerodynamic characteristics of the model, presented in figure 7 for both control configurations at $M = 0.75$, are representative of the basic data plots obtained in this investigation. Figure 8 presents plots of the rolling-moment coefficients and the increments in lift and pitching-moment coefficients due to deflection against control deflection for representative Mach numbers throughout the range from 0.75 to 1.96. In this figure, the signs of the test values of angle of attack, control deflection, and model force and moment coefficients obtained at negative angles of attack have been arbitrarily reversed for convenience of presentation. This reversal was permissible because of the model symmetry. The hinge-moment characteristics as a function of both angle of attack and deflection are presented for the unbalanced control in figure 9 and for the 100-percent overhang balanced control in figure 10.

Rolling-moment corrections for reflection-plane effects at transonic Mach numbers are unknown. The rolling-moment data, however, are presented at all test Mach numbers for the sake of completeness. The discussion of control characteristics at subsonic Mach numbers, therefore, is confined to lift and pitching moment. At Mach numbers above $M = 1.09$, no reflection-plane corrections are required.

Control effectiveness.- For the unbalanced flap, ΔC_L and ΔC_m increased with increasing control deflection at all Mach numbers throughout the angle-of-attack range of the tests (fig. 8). The variations of ΔC_L and ΔC_m with deflection were essentially linear except at subsonic Mach numbers where the slopes of the curves $\Delta C_{L\delta}$ and $\Delta C_{m\delta}$ decreased about 65 percent with an increase in deflection beyond $\pm 8^\circ$. Increases in angle of attack, if anything, tended to increase the effectiveness of the control at all Mach numbers except near $M = 1.0$ where the reverse occurred.

Moving the hinge line back to the control midchord line, in general, caused large decreases in effectiveness. An exception may be noted for small deflections at Mach numbers 0.75 and 0.865 where $\Delta C_{L\delta}$ and $\Delta C_{m\delta}$ were only slightly less for the balanced control than for the unbalanced control. At Mach numbers above 0.865, the difference in effectiveness

of the two controls even at small deflections was large; values of $C_{l\delta}$, $\Delta C_{L\delta}$, and $\Delta C_{m\delta}$ for the balanced control were less than 50 percent of those of the unbalanced control at supersonic speeds. At subsonic speeds, severe breaks occurred in the ΔC_L and ΔC_m curves at approximately the deflection for which the control unported (the deflection for which the control chord plane no longer intersects the wing, 8°). Further increases in positive deflection caused little change in values of ΔC_L or ΔC_m . At large negative deflections, positive slopes ($\Delta C_{L\delta}$ and $\Delta C_{m\delta}$) indicate the control has regained some of its effectiveness and in the case of a lateral control may partially offset the losses at positive deflections. At supersonic speeds no large effects of unporting were evidenced. However, at angles of attack other than zero, the slopes $C_{l\delta}$, $\Delta C_{L\delta}$, and $\Delta C_{m\delta}$ decreased with increasing deflection above about 10° . Above about 20° , further increases in deflection resulted in decreases in values of C_l , ΔC_L , and ΔC_m . These decreases were more severe above $M = 1.25$ and reversals in sign of C_l and ΔC_L occurred at the largest angle of attack between 30° and 40° deflection. At negative deflections, the balanced control showed losses in effectiveness only at zero angle of attack and, as was the case at subsonic speeds, for a lateral control may partially offset the losses at positive deflections.

Control hinge moments.- For the unbalanced control, the hinge-moment variation with deflection curves (figs. 9(a) and 9(b)) were essentially linear through zero deflection for nearly all angles of attack and had negative slopes. The linear range extended to about 20° deflection at Mach numbers 0.75 and 0.865 and to about 10° at higher Mach numbers. At larger deflections the slopes became less negative and the curves were again nearly linear up to the largest deflections of the tests (40°). The hinge-moment variation with angle of attack for the unbalanced control (figs. 9(c) and 9(d)) was not markedly affected by changes in control deflection and was for the most part linear with negative slopes throughout the Mach number range of the tests. At subsonic Mach numbers $C_{h\alpha}$ was small but then increased with increasing Mach numbers in the transonic range. (See also fig. 4.)

It is of interest to compare the hinge-moment parameters $C_{h\alpha}$ and $C_{h\delta}$ for the unbalanced control at supersonic speeds with the results of theory and with results of tests of a somewhat similar model made in the Ames 6- by 6-foot supersonic tunnel (fig. 4) and also to consider the effects of control area at the wing tip on these parameters. Theoretical values of $C_{h\alpha}$ and $C_{h\delta}$ for the model tested in the Ames 6- by 6-foot tunnel were taken from reference 2. Theoretical values of $C_{h\delta}$ for the present model were obtained from the equations of

reference 11 and theoretical values of $C_{h\alpha}$ were obtained from equations in the appendix. All theoretical curves were based on linear theory and thickness effects were not considered. The addition of the tip caused a sizable increase in both $C_{h\alpha}$ and $C_{h\delta}$ as shown by both experiment and theory. Experimental values were about 75 percent of theoretical values for all cases.

Setting the control hinge line back to the midchord line gave variations of hinge moment with deflection that were nonlinear for most of the deflection range (fig. 10). At subsonic Mach numbers the slopes through zero deflection were positive and indicated an overbalanced condition but then decreased rapidly with increasing Mach numbers and were negative at all Mach numbers above 1.05 (see also fig. 5). At subsonic Mach numbers rather severe reversals in the slopes of the curves occurred at deflections close to that at which the control unported. The overbalancing moments at small deflections are associated with the high pressure peak inherent in the loading at the nose of the control ahead of the hinge line. It may be that, as the control unports, flow separation over the upper surface of the control reduces the peak pressures and thereby reduces the control overbalance. This reason would also help explain the previously mentioned losses in lift and pitching moment due to deflection which occurred when the control unported. At supersonic speeds, the negative slopes at small deflections may be attributed to the overhang balance operating in the wake of the wing as was shown in reference 5. Figure 10 shows that, at supersonic speeds as the control unported, the overhang balance became effective and the control hinge moments due to deflection remained constant or decreased with increasing deflection up to about 20° . At higher deflections for positive angles of attack the hinge moments again increased negatively with increasing deflection. For negative angles of attack the situation was reversed and the control hinge moments increased positively and became overbalanced at the largest deflections. These variations at largest deflections are apparently an effect of angle of attack as shown by the severe nonlinearities in figures 10(a) and 10(b). Figures 10(c) and 10(d) show that moving the hinge line back to midchord does a reasonably good job of balancing C_h due to angle of attack at Mach numbers greater than unity, except at high deflection angles and at Mach numbers less than unity tends to overbalance C_h due to angle of attack.

Figures 11 and 12 have been prepared to aid the evaluation of the hinge-moment characteristics of the two controls. Values of C_l required to produce a roll rate of the subject wing of 3.5 radians per second (a 30-foot wing span being assumed at an altitude of 40,000 feet) were calculated by use of theoretical values of C_{lp} from references 12 and 13. Figure 11 presents the experimental values of $C_h \left(\frac{c_f}{c_t} \right)^2$ against Mach number for equal up and down deflections of opposite ailerons which

would produce the calculated required rolling moment. The parameter $C_h \left(\frac{c_f}{c_t} \right)^2$ is used in this figure to afford a direct comparison of the hinge moments for the two controls. Data are shown for the steady-roll and static cases. Data for the static case are representative of the case in which the controls are fully deflected before the aircraft starts to roll. The analysis by which these data were obtained is discussed in reference 14. Values of $C_h \left(\frac{c_f}{c_t} \right)^2$ for both controls are compared at $\alpha = 0^\circ$ and $\alpha = 6^\circ$ in figure 11. Differences between subsonic and supersonic values of the parameter are considerably smaller for the balanced control than for the unbalanced control at both angles of attack. Figure 11 also shows that the hinge moments of the balanced control are much smaller in magnitude than those of the unbalanced control throughout the speed range of the tests. Correspondingly less torque would be required to be available at the control and the strength and weight of the actuating mechanism could be reduced.

Although hinge moments are important as such for the preceding reasons, the work required to overcome the hinge moments due to deflection is an important consideration because it determines the amount of energy that must be supplied to a power-boost system. A comparison on the basis of deflection work for the two controls producing the above roll rate is presented, for supersonic speeds, in figure 12. These data indicate that advantages at supersonic speeds of the balanced control over the unbalanced control, although still large at zero angle of attack, are considerably reduced at an angle of attack of 8° .

SUMMARY OF RESULTS

An investigation of a 60° delta wing equipped with an unbalanced and a 100-percent overhang balanced constant-chord control in the Langley 9- by 12-inch blowdown tunnel at Mach numbers from 0.75 to 1.96 indicated the following results:

The unbalanced control was effective throughout the range of the investigation including angles of attack of $\pm 12^\circ$ and deflections of $\pm 40^\circ$. At small deflections, the balanced control was only slightly less effective in causing changes in lift and pitching-moment coefficients than the unbalanced control at subsonic Mach numbers but was less than 50 percent as effective at supersonic Mach numbers. The effectiveness of the balanced control at positive angles of attack and deflection was lost soon after the control unported (at a deflection angle of approximately 8°) at subsonic Mach numbers and above about 15° to 20° deflection at supersonic Mach numbers.

The balance area of the setback hinge-line control had strong overbalancing effects on the hinge-moment coefficients due to deflection at subsonic speeds until the control unported but was much less effective thereafter. At supersonic Mach numbers, however, the balance area was relatively ineffective until after the control unported. The resulting nonlinearities in the curves of the hinge moment against deflection angle were most severe at low deflections at Mach numbers less than 1.0 and at high deflections at Mach numbers greater than 1.0. The variation of hinge moment with angle of attack was overbalanced at subsonic Mach numbers and reasonably well balanced at supersonic Mach numbers except at high deflections.

At moderate angles of attack with the controls deflected to produce a given roll rate the magnitude of the hinge moments were much smaller for the balanced control and showed less change with Mach number than that for the unbalanced control. Comparison on the basis of deflection work for the same roll rate, however, showed somewhat less advantage to the balanced control at moderate angles of attack for supersonic speeds.

Comparison of control characteristics for the present model with data obtained for nearly similar models in larger facilities presents strong justification for the technique of testing shimmed semispan models of practical size at transonic speeds in the slotted nozzle.

Langley Aeronautical Laboratory,
National Advisory Committee for Aeronautics,
Langley Field, Va., June 30, 1954.

APPENDIX

DERIVATIONS AND FORMULAS FOR $C_{h\alpha}$

Reference 11 treats the problem of two types of constant-chord partial-span flaps; one extending outboard from the center of the wing and the other extending inboard from the tip of the wing. The full-span flap is, of course, a special case of the latter type. The present report is concerned with the type of partial-span flap that does not necessarily extend to either the center of the wing or to the wing tip (see fig. 13).

The characteristics due to deflection of the type of partial-span flap of the present report may be obtained with little difficulty from the equations given in reference 11 for the type flap which extends outboard from the center of the wing and need not be considered here. The derivations and formulas for $C_{h\alpha}$ that follow are restricted to the case where the Mach line from the wing apex is ahead of the wing leading edge and are subject to all the limitations of the linearized theory.

If the pressure distribution due to angle of attack is known, $C_{h\alpha}$ can be found by integrating the pressure over the proper areas, multiplying by the correct moment arms, and dividing by the proper dimensions to form coefficients.

The local pressure difference between upper and lower surface of a triangular wing due to angle of attack is given in references 11 and 13. This pressure is given in nondimensional form, with proper changes in notation, by the following relationship:

$$\frac{C_P}{\alpha} = \frac{P}{q\alpha} = \frac{K}{\sqrt{k^2 - t^2}}$$

where

$$K = \frac{4k^2}{E'(m)}$$

and $E'(m)$ is the complete elliptic integral of second kind with modulus $\sqrt{1 - m^2}$. Other symbols are defined in figure 13.

This expression can be integrated over a triangular segment of the wing, such as shown in figure 10, to give the average pressure of the segment and the location of the ray on which the center of pressure of the segment lies. For example, the average pressure coefficient for triangular segment I is found from

$$\frac{C_{P_{av}}}{\alpha} (I) = \frac{\int_{1/t_1}^{1/t_2} \frac{K}{\sqrt{k^2 - t^2}} d\left(\frac{1}{t}\right)}{\int_{1/t_1}^{1/t_2} d\left(\frac{1}{t}\right)}$$

to be

$$\frac{C_{P_{av}}}{\alpha} (I) = \frac{K}{k^2(1-a)} \left(\sqrt{k^2 - t_2^2} - a \sqrt{k^2 - \frac{t_2^2}{a^2}} \right)$$

where $t_1 = \frac{t_2}{a}$ and $a = 1 - \frac{c_f}{c_r}$. The length of the moment arm about the apex of the wing may be expressed by

$$\frac{\bar{x}}{c_f} (I) = \frac{-2c_r t_2}{3c_f} \frac{1}{t_{cp}(I)}$$

where t_{cp} is found from

$$\frac{1}{t_{cp}} (I) = \frac{\int_{1/t_1}^{1/t_2} \frac{1}{t} \frac{K}{\sqrt{k^2 - t^2}} d\left(\frac{1}{t}\right)}{\int_{1/t_1}^{1/t_2} \frac{K}{\sqrt{k^2 - t^2}} d\left(\frac{1}{t}\right)}$$

to be

$$\frac{1}{t_{cp}} (I) = \frac{\frac{1}{2} \left[\frac{1}{t_2} \sqrt{k^2 - t_2^2} - \frac{a^2}{t_2} \sqrt{k^2 - \frac{t_2^2}{a^2}} + \frac{t_2}{k} \left(\cosh^{-1} \frac{k}{t_2} - \cosh^{-1} \frac{ak}{t_2} \right) \right]}{\sqrt{k^2 - t_2^2} - a \sqrt{k^2 - t_1^2}}$$

The moment of the triangular segment I about the wing apex reduced on the basis of the flap area is then

$$\frac{1}{S_f c_f} \left(\frac{C_{p_{av}}}{\alpha} S' \bar{x} \right)_I = \frac{-K c_r^3 t_2^2}{6 b_f c_f^2 k^3} \left[\frac{k}{t_2} \sqrt{k^2 - t_2^2} - \frac{a^2 k}{t_2} \sqrt{k^2 - \frac{t_2^2}{a^2}} + t_2 \left(\cosh^{-1} \frac{k}{t_2} - \cosh^{-1} \frac{ka}{t_2} \right) \right]$$

Similarly, the hinge-moment parameter $\frac{C_{p_{av}}}{\alpha} \frac{S'}{S_f} \frac{\bar{x}}{c_f}$ may be found for the other regions of integration of figure 10. From

$$C_{h_\alpha} = \left[\left(\frac{C_{p_{av}}}{\alpha} S' \bar{x} \right)_I + \left(\frac{C_{p_{av}}}{\alpha} S' \bar{x} \right)_{II} - \left(\frac{C_{p_{av}}}{\alpha} S' \bar{x} \right)_{III} - \left(\frac{C_{p_{av}}}{\alpha} S' \bar{x} \right)_{IV} \right] \frac{1}{S_f c_f} - \left[\left(\frac{C_{p_{av}}}{\alpha} \frac{S'}{S_f} \right)_I + \left(\frac{C_{p_{av}}}{\alpha} \frac{S'}{S_f} \right)_{II} - \left(\frac{C_{p_{av}}}{\alpha} \frac{S'}{S_f} \right)_{III} - \left(\frac{C_{p_{av}}}{\alpha} \frac{S'}{S_f} \right)_{IV} \right] \frac{x_h}{c_f}$$

the final expression is found to be

$$\begin{aligned}
 C_{h\alpha} = & \frac{-Kc_r^3}{3b_f c_f^2} \left[\frac{(1-3a)t_2}{2k^2} \sqrt{k^2 - t_2^2} + \frac{t_2 a^2}{k^2} \sqrt{k^2 - \frac{t_2^2}{a^2}} - \frac{(1-3a)t_4}{2k^2} \sqrt{k^2 - t_4^2} - \right. \\
 & \frac{t_4 a^2}{k^2} \sqrt{k^2 - \frac{t_4^2}{a^2}} + \frac{t_2^3}{2k^3} \left(\cosh^{-1} \frac{k}{t_2} - \cosh^{-1} \frac{ka}{t_2} \right) - \\
 & \frac{t_4^3}{2k^3} \left(\cosh^{-1} \frac{k}{t_4} - \cosh^{-1} \frac{ka}{t_4} \right) + \left(1 - \frac{3a}{2} \right) \left(\sin^{-1} \frac{t_2}{k} - \sin^{-1} \frac{t_4}{k} \right) + \\
 & \left. \frac{a^3}{2} \left(\sin^{-1} \frac{t_2}{ka} - \sin^{-1} \frac{t_4}{ka} \right) \right]
 \end{aligned}$$

REFERENCES

1. Axelson, John A.: A Summary and Analysis of Wind-Tunnel Data on the Lift and Hinge-Moment Characteristics of Control Surfaces Up to a Mach Number of 0.90. NACA RM A7L02, 1947.
2. Boyd, John W., and Pfyl, Frank A.: Experimental Investigation of Aerodynamically Balanced Trailing-Edge Control Surfaces on an Aspect Ratio 2 Triangular Wing at Subsonic and Supersonic Speeds. NACA RM A52L04, 1953.
3. Lockwood, Vernard E., and Hagerman, John R.: Aerodynamic Characteristics at Transonic Speeds of a Tapered 45° Sweptback Wing of Aspect Ratio 3 Having a Full-Span Flap Type of Control With Overhang Balance. Transonic-Bump Method. NACA RM L51L11, 1952.
4. Stone, David G.: Recent Data on Controls. NACA RM L52A10, 1952.
5. Mueller, James N.: An Investigation at Mach Number 2.40 of Flap-Type Controls Equipped With Overhang Nose Balances. NACA RM L53I21, 1953.
6. Thompson, Robert F.: Hinge-Moment, Lift, and Pitching-Moment Characteristics of a Flap-Type Control Surface Having Various Hinge-Line Locations on a 4-Percent-Thick, 60° Delta Wing. Transonic-Bump Method. NACA RM L54B08, 1954.
7. Burgess, Warren C., Jr., and Seashore, Ferris L.: Criteria for Condensation-Free Flow in Supersonic Tunnels. NACA TN 2518, 1951.
8. May, Ellery B., Jr.: Investigation of the Effects of Leading-Edge Chord-Extensions on the Aerodynamic and Control Characteristics of Two Sweptback Wings at Mach Numbers of 1.41, 1.62, and 1.96. NACA RM L50L06a, 1951.
9. Schulze, Wallace M., Ashby, George C., Jr., and Erwin, John R.: Several Combination Probes for Surveying Static and Total Pressure and Flow Direction. NACA TN 2830, 1952.
10. Conner, D. William: Aerodynamic Characteristics of Two All-Movable Wings Tested in the Presence of a Fuselage at a Mach Number of 1.9. NACA RM L8H04, 1948.
11. Tucker, Warren A., and Nelson, Robert L.: Theoretical Characteristics in Supersonic Flow of Two Types of Control Surfaces on Triangular Wings. NACA Rep. 939, 1949. (Supersedes NACA TN's 1600, 1601, and 1660.)

12. Polhamus, Edward C.: A Simple Method of Estimating the Subsonic Lift and Damping in Roll of Sweptback Wings. NACA TN 1862, 1949.
13. Malvestuto, Frank S., Jr., Margolis, Kenneth, and Ribner, Herbert S.: Theoretical Lift and Damping in Roll at Supersonic Speeds of Thin Sweptback Tapered Wings With Streamwise Tips, Subsonic Leading Edges, and Supersonic Trailing Edges. NACA Rep. 970, 1950. (Supersedes NACA TN 1860.)
14. Goin, Kenneth L., and Palmer, William E.: Subsonic and Supersonic Hinge-Moment and Effectiveness Characteristics of an Unbalanced Lateral Control Having Low Theoretical Hinge Moments at Supersonic Speeds. NACA RM L53G31a, 1953.
15. Stephenson, Jack D., and Ameudo, Arthur R.: Tests of a Triangular Wing of Aspect Ratio 2 in the Ames 12-Foot Pressure Wind Tunnel. II - The Effectiveness and Hinge Moments of a Constant-Chord Plain Flap. NACA RM A8E03, 1948.
16. Mitcham, Grady L., Stevens, Joseph E., and Norris, Harry P.: Aerodynamic Characteristics and Flying Qualities of a Tailless Triangular-Wing Airplane Configuration As Obtained From Flights of Rocket-Propelled Models at Transonic and Low Supersonic Speeds. NACA RM L9L07, 1950.
17. Wolhart, Walter D., and Michael, William H., Jr.: Wind-Tunnel Investigation of the Low-Speed Longitudinal and Lateral Control Characteristics of a Triangular-Wing Model of Aspect Ratio 2.31 Having Constant-Chord Control Surfaces. NACA RM L50G17, 1950.

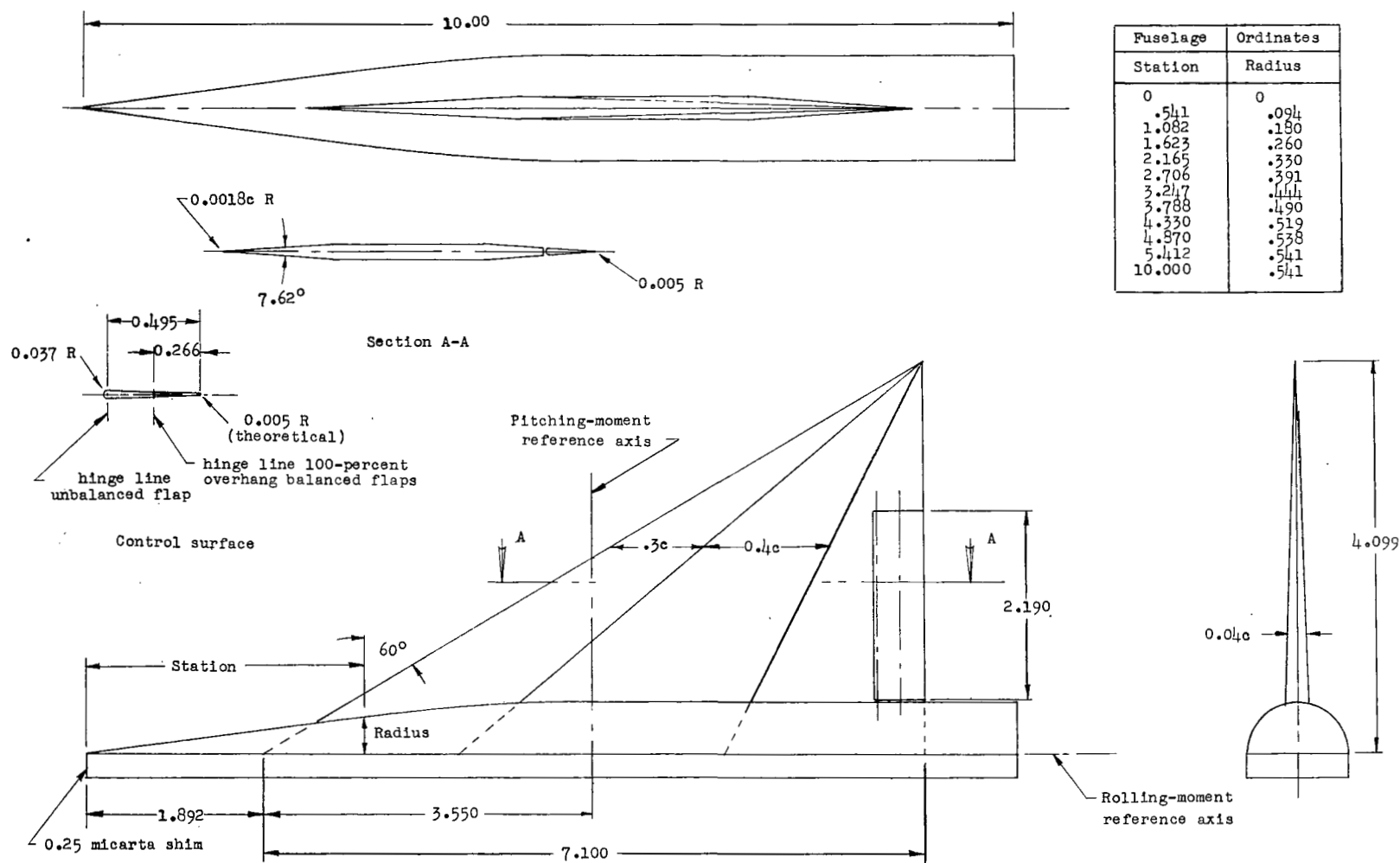


Figure 1.- Details of semispan-wing-fuselage combination, mean aerodynamic chord, 4.733 inches; semispan, 4.099 inches; half-wing area, 14.552 square inches. All dimensions are in inches unless otherwise noted.

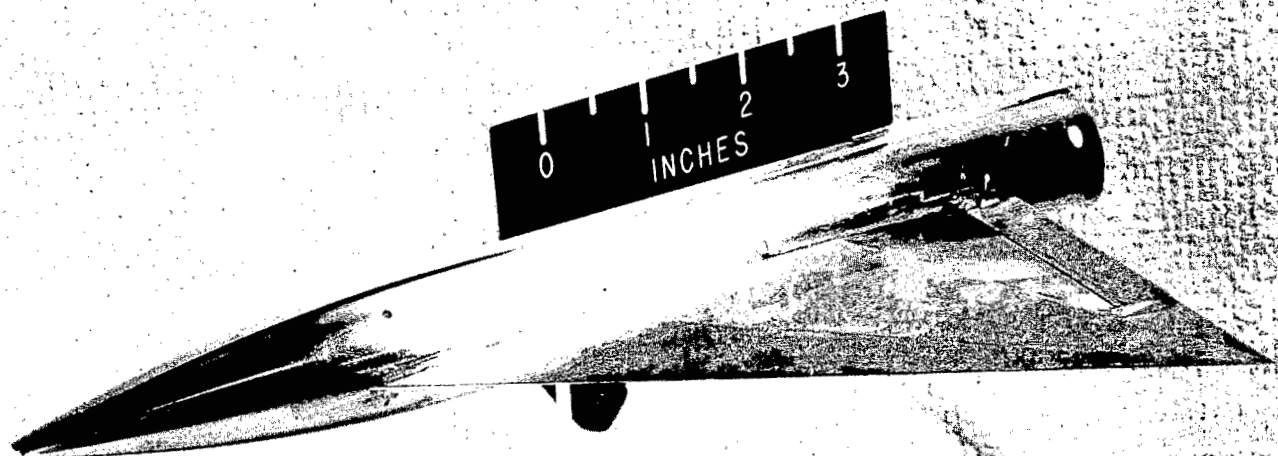
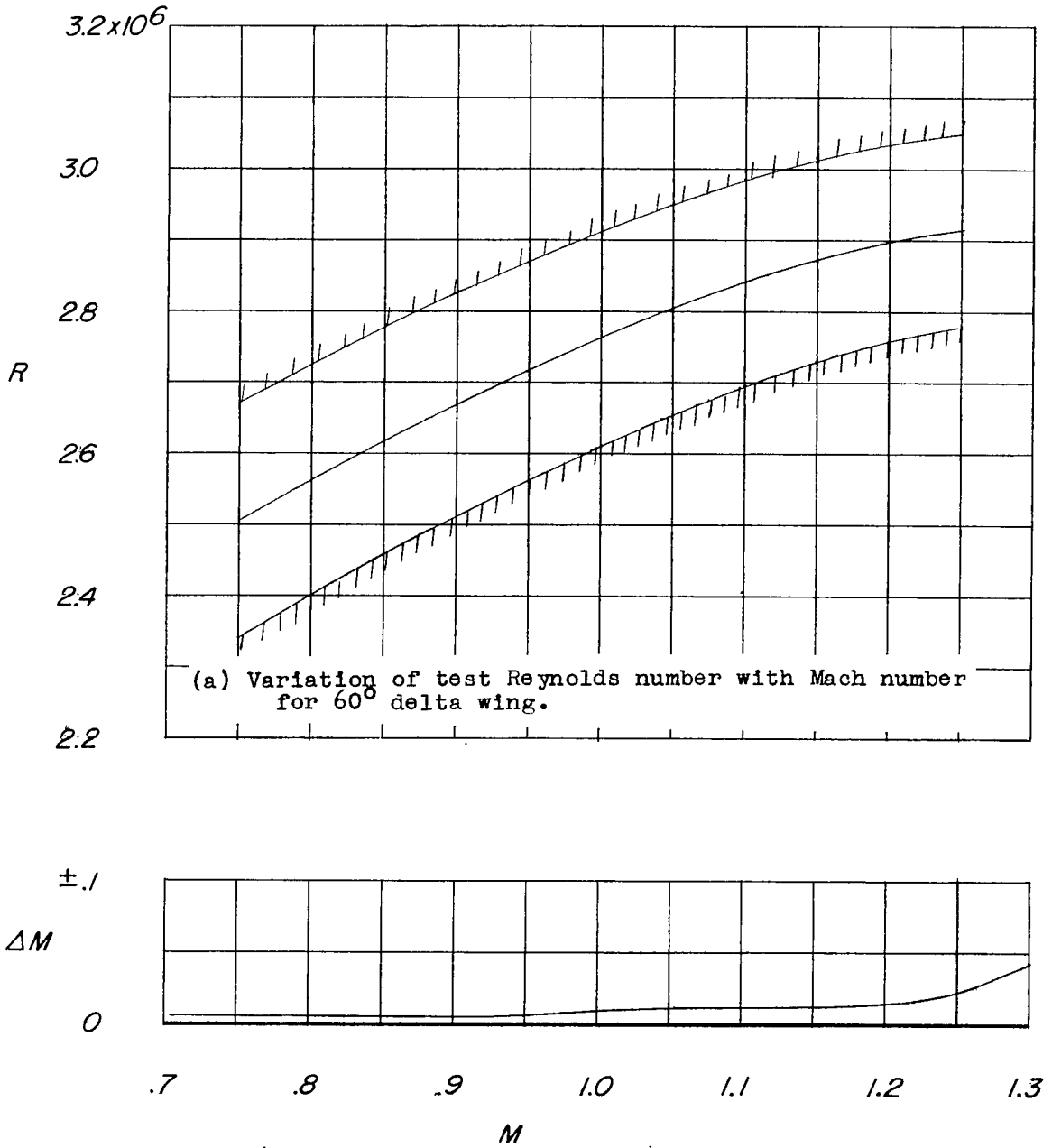


Figure 2.- Photograph of model with 100-percent overhang balanced flap.

L-82705



(b) Maximum deviation from average test section Mach number.

Figure 3.- Variation of Mach number and Reynolds number in transonic nozzle.

Line key	Control	Test facility	Source of data	$\frac{c_t}{c_r}$	$\frac{S_f}{S}$	L.E. sweepback	Airfoil section	Reynolds number	ϕ
○—	Tip off	9- by 12-inch blowdown tunnel	Present report	0.0698	0.0763	60°	Modified double wedge	2.4 to 3.0 × 10 ⁶	6°
□—	Horn off	6- by 6-foot supersonic tunnel	Ref. 2	.0646	.0926	63.43°	0005-63	4.4 × 10 ⁶	6.7°
- - -	Horn off	12-foot pressure tunnel	Ref. 15	.1056	.1699	63.03°	Double wedge	5.3 × 10 ⁶	3.6°
- - -	Horn on	Rocket powered model	Ref. 16	.1125	.1376	60°	65(06)-006.5	10 to 20 × 10 ⁶	4.8°
● ○ □	Tip off Horn off Horn on	Stability tunnel	Ref. 17	.1123	.1372 .1376 .1376	60°	65(06)-006.5	2.06 × 10 ⁶	8°

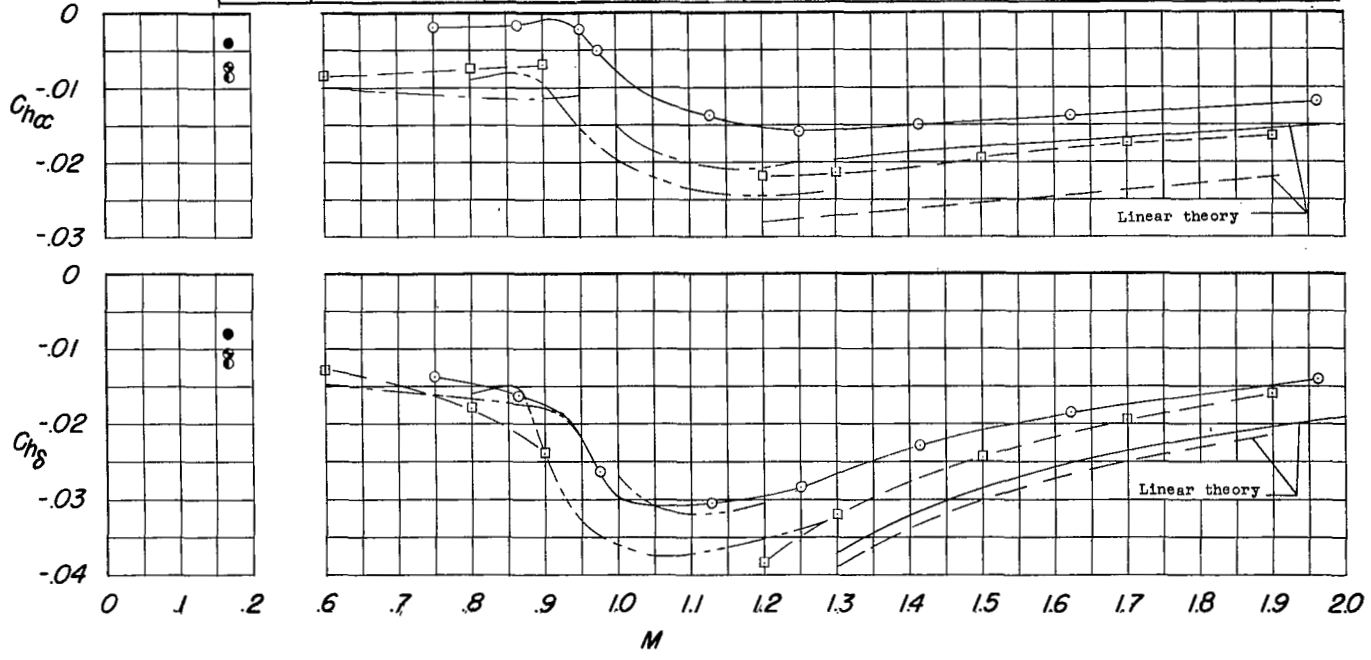


Figure 4.- Comparison of the variation with Mach number of $C_{h\alpha}$ and $C_{h\delta}$ ($\delta = 0^\circ$, $\alpha = 0^\circ$) for unbalanced constant-chord flap-type controls of several models.

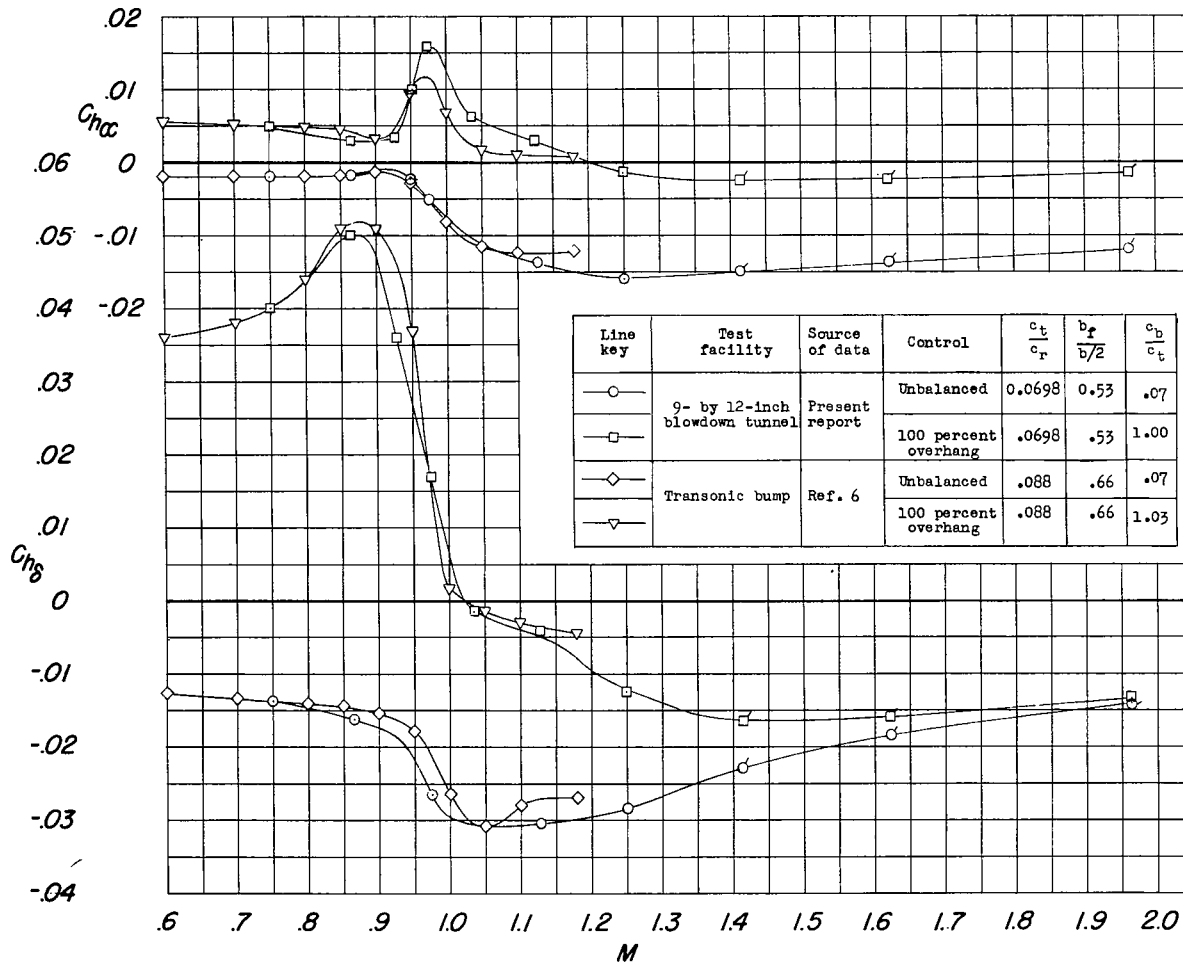
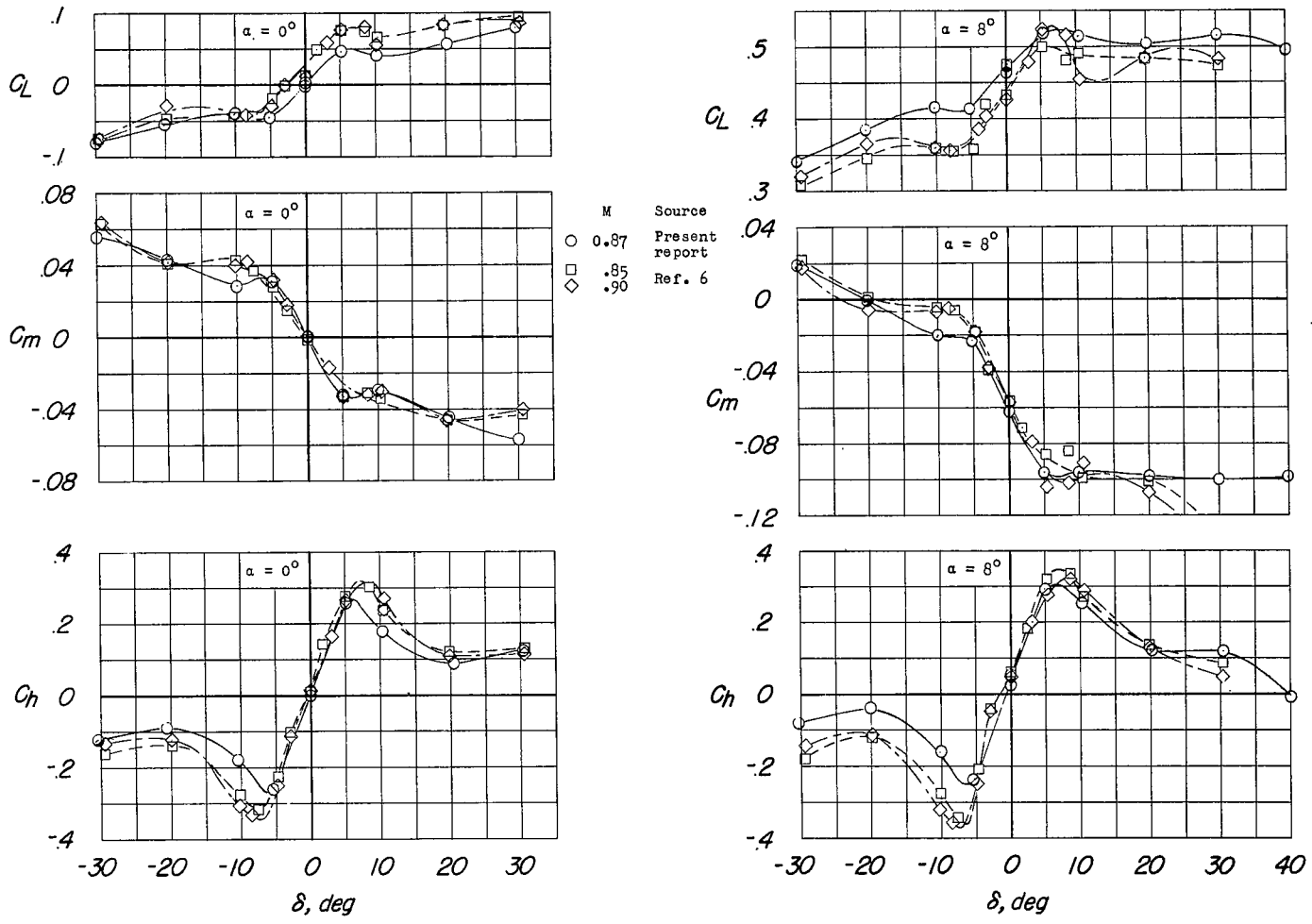
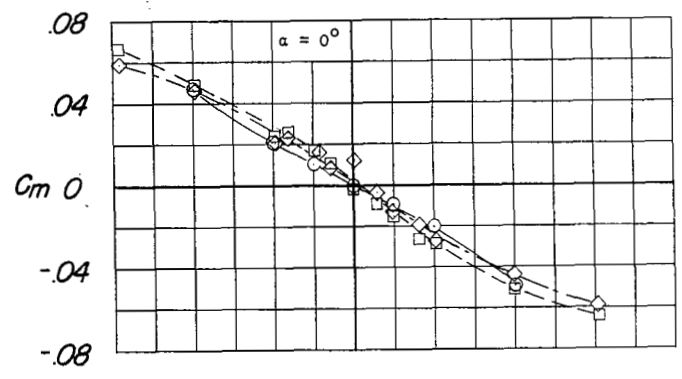
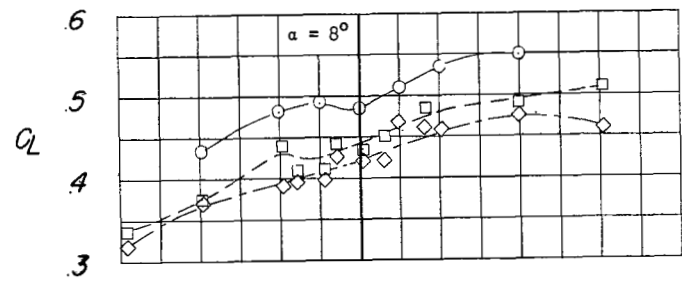
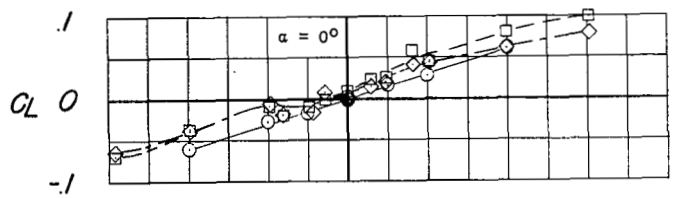


Figure 5.- Comparison of the variation with Mach number of $C_{h\alpha}$ and $C_{h\delta}$ ($\delta = 0^\circ$ and $\alpha = 0^\circ$, respectively) for constant-chord flap-type controls of several models. Flagged symbols denote data obtained in fixed Mach number nozzles.

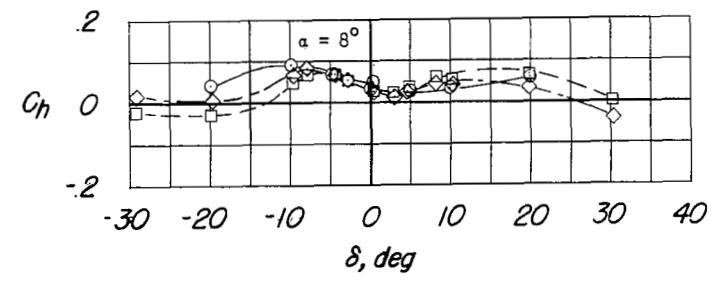
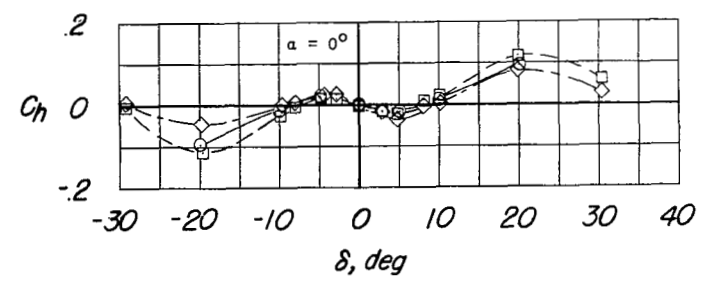
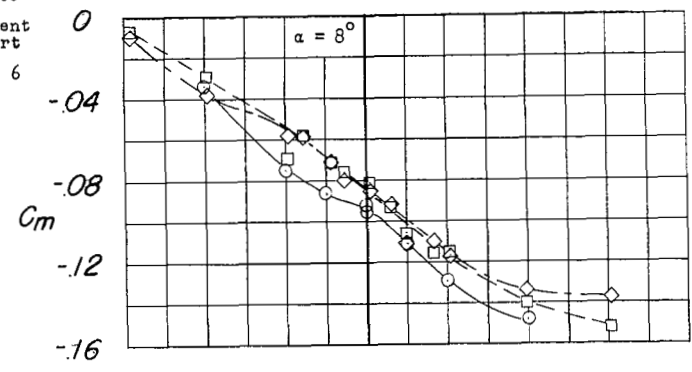


(a) $M \approx 0.9$.

Figure 6.- Comparison of the variation with control deflection of the lift, pitching-moment, and hinge-moment coefficients for 100-percent balanced controls of two models.

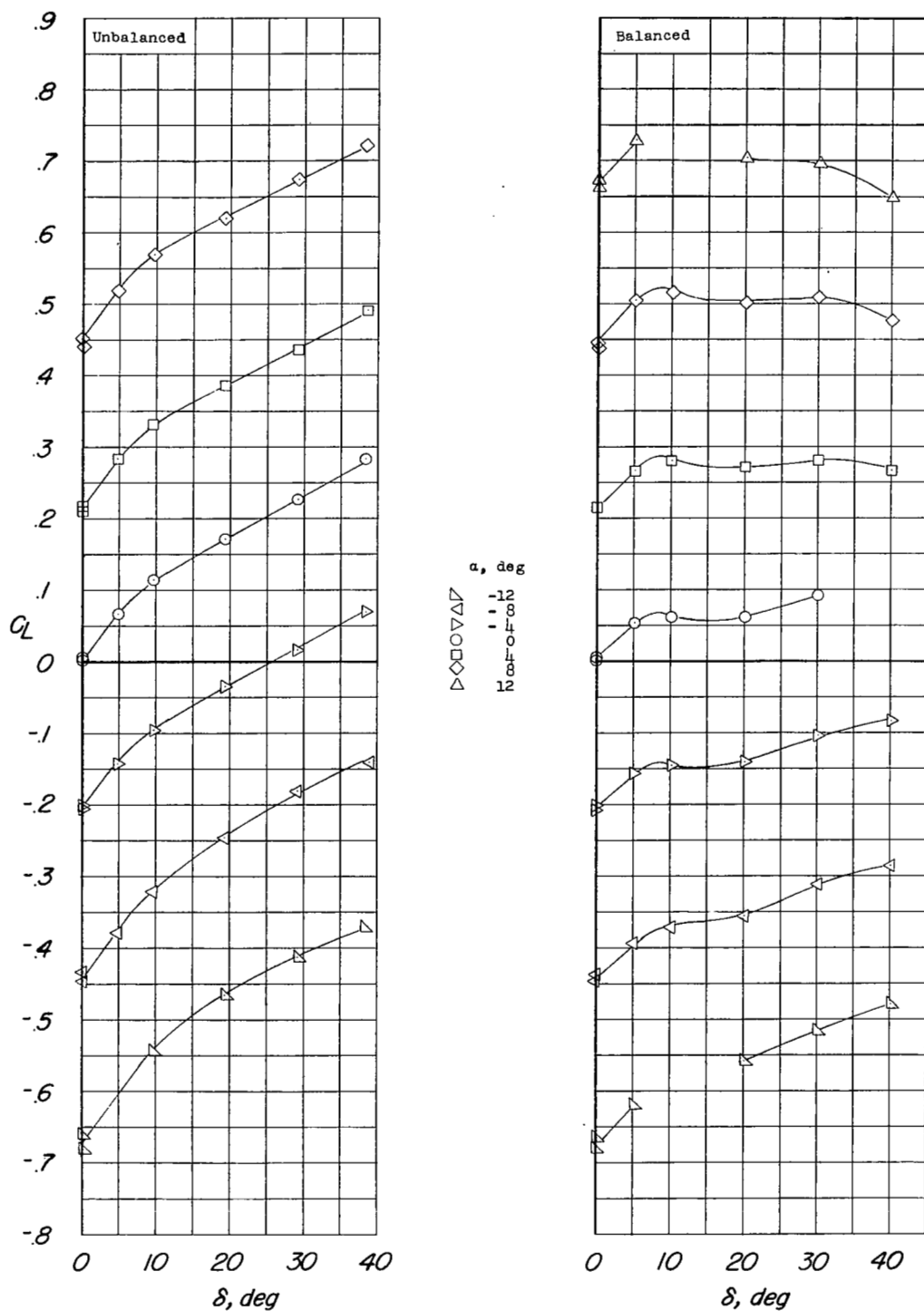


M Source
 ○ 1.13 Present report
 □ 1.10 Ref. 6
 ◇ 1.18



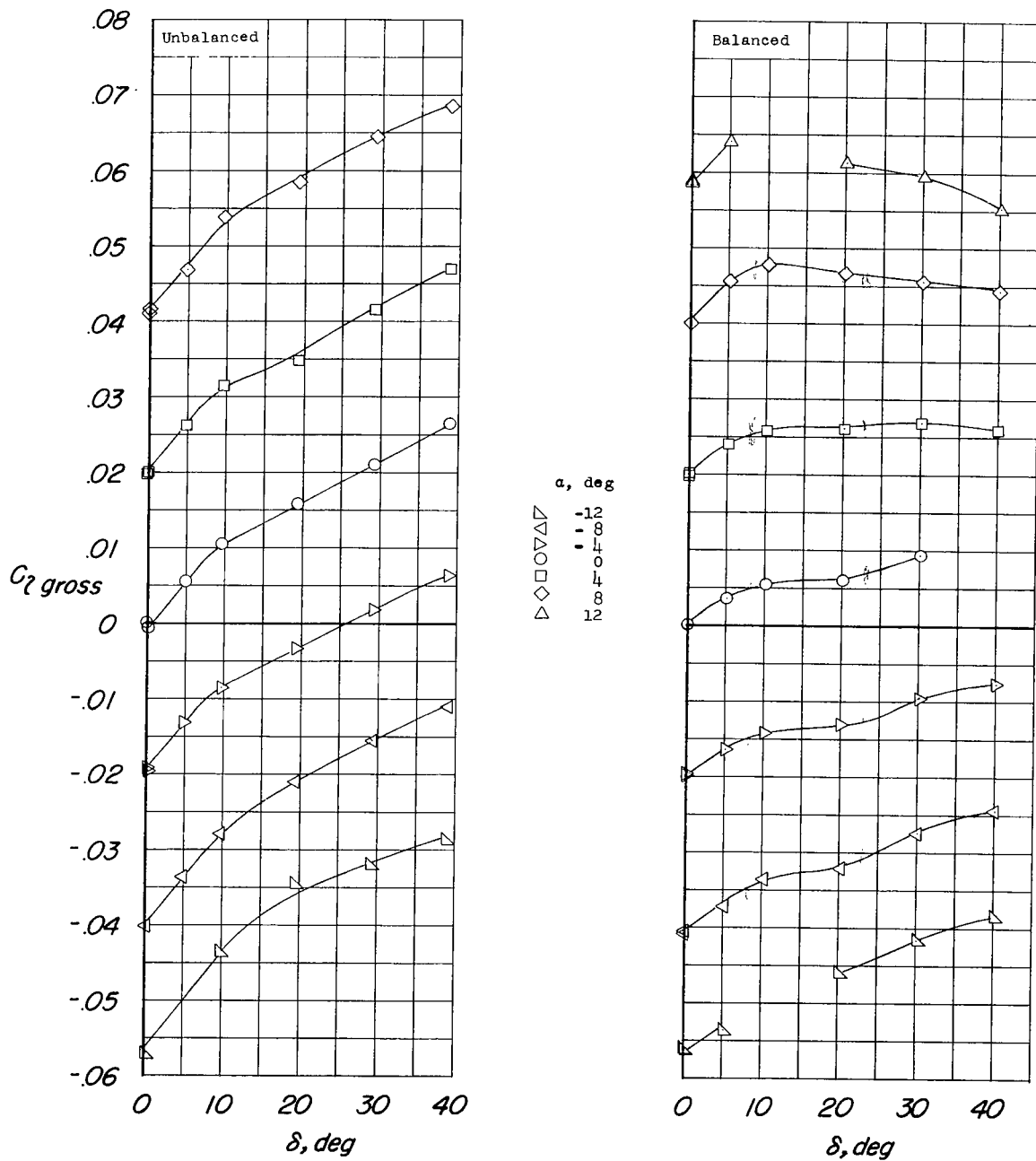
(b) $M \approx 1.15$.

Figure 6.- Concluded.



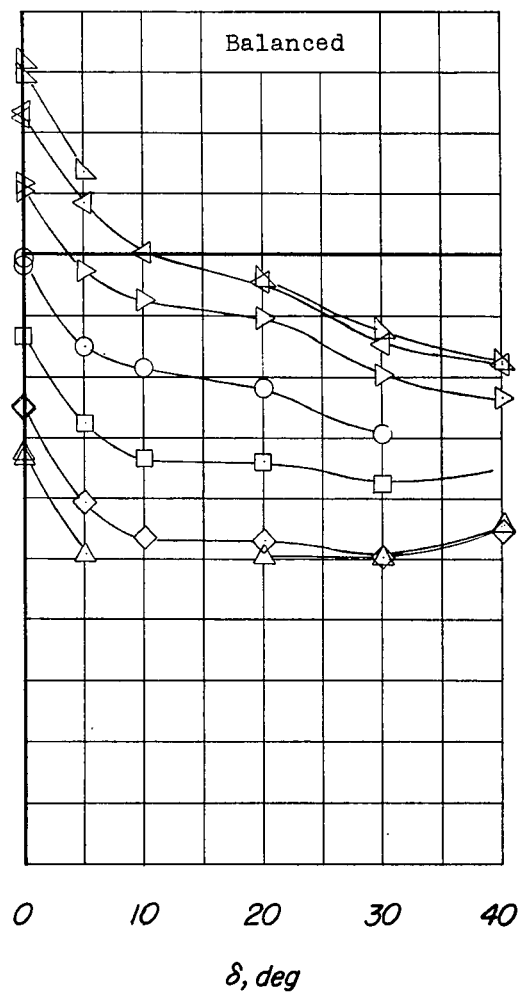
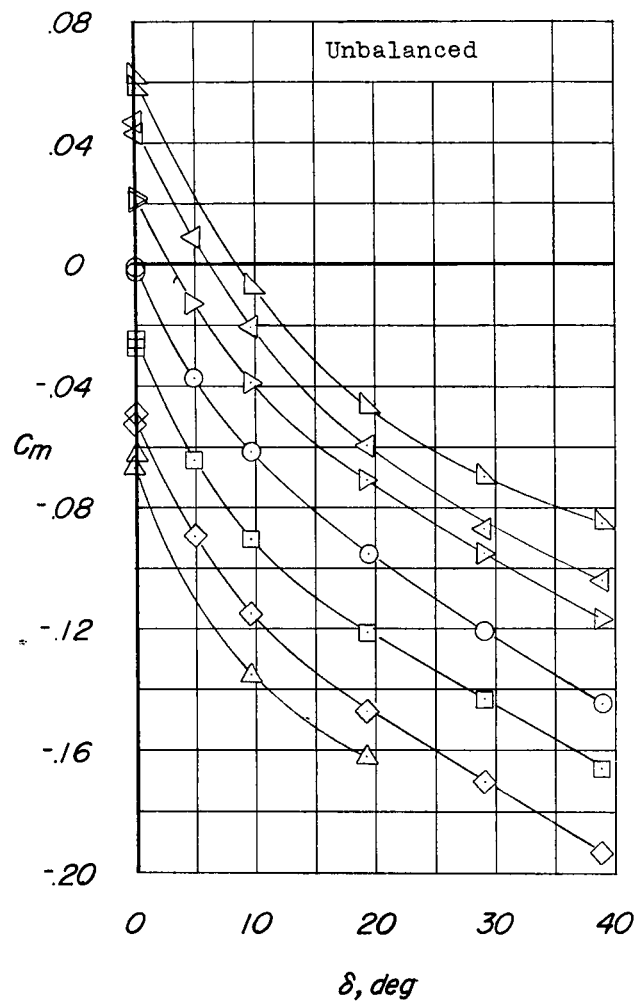
(a) C_L against δ .

Figure 7.- Aerodynamic characteristics of a semispan-delta-wing-fuselage combination with two constant-chord trailing-edge controls. $M = 0.75$.



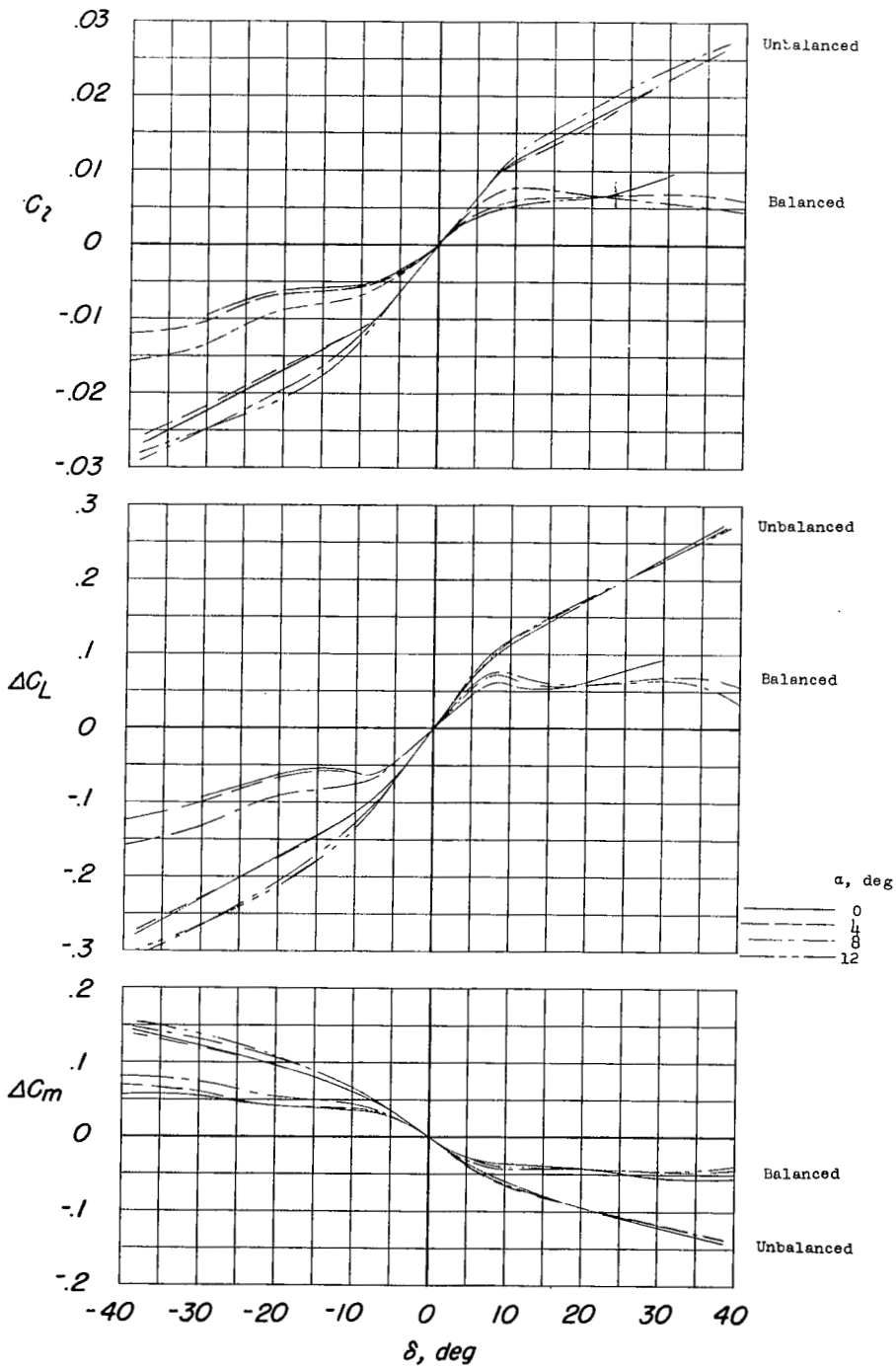
(b) $C_{l_{gross}}$ against δ .

Figure 7.- Continued.



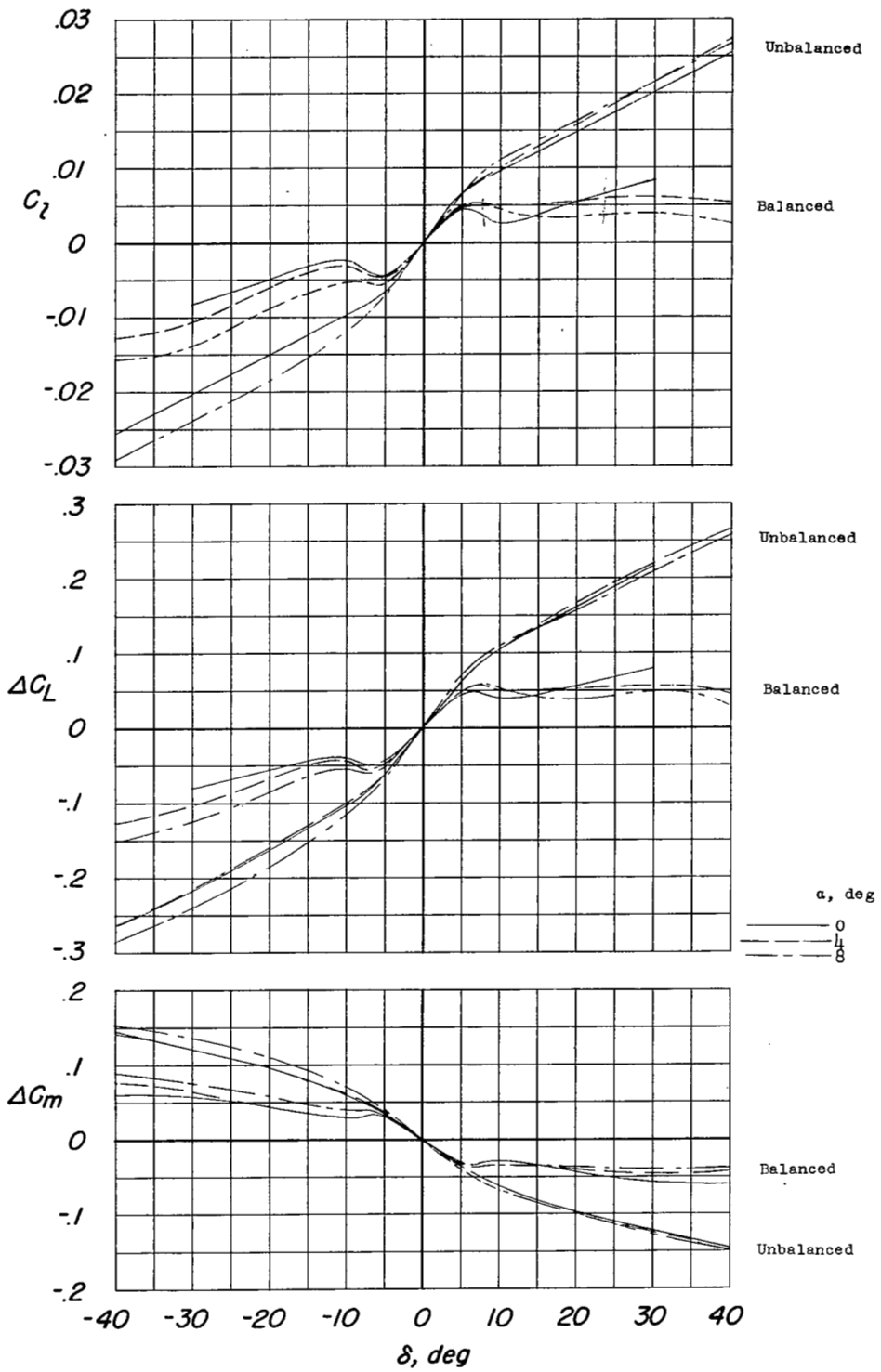
(c) C_m against δ .

Figure 7.- Concluded.



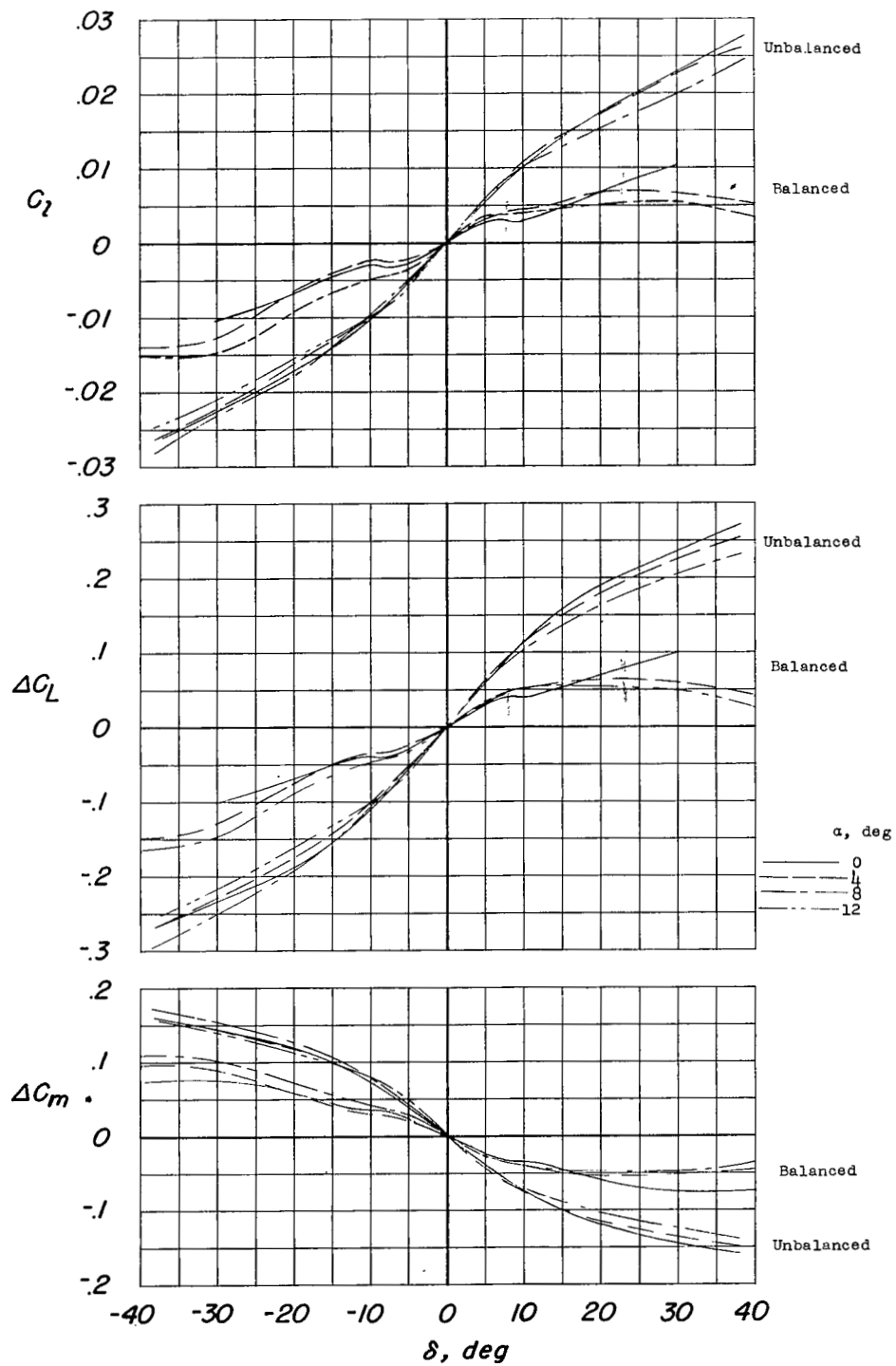
(a) $M = 0.75$.

Figure 8.- The variation with control deflection of rolling moment and increments of lift and pitching moment due to deflection at various angles of attack for two controls.



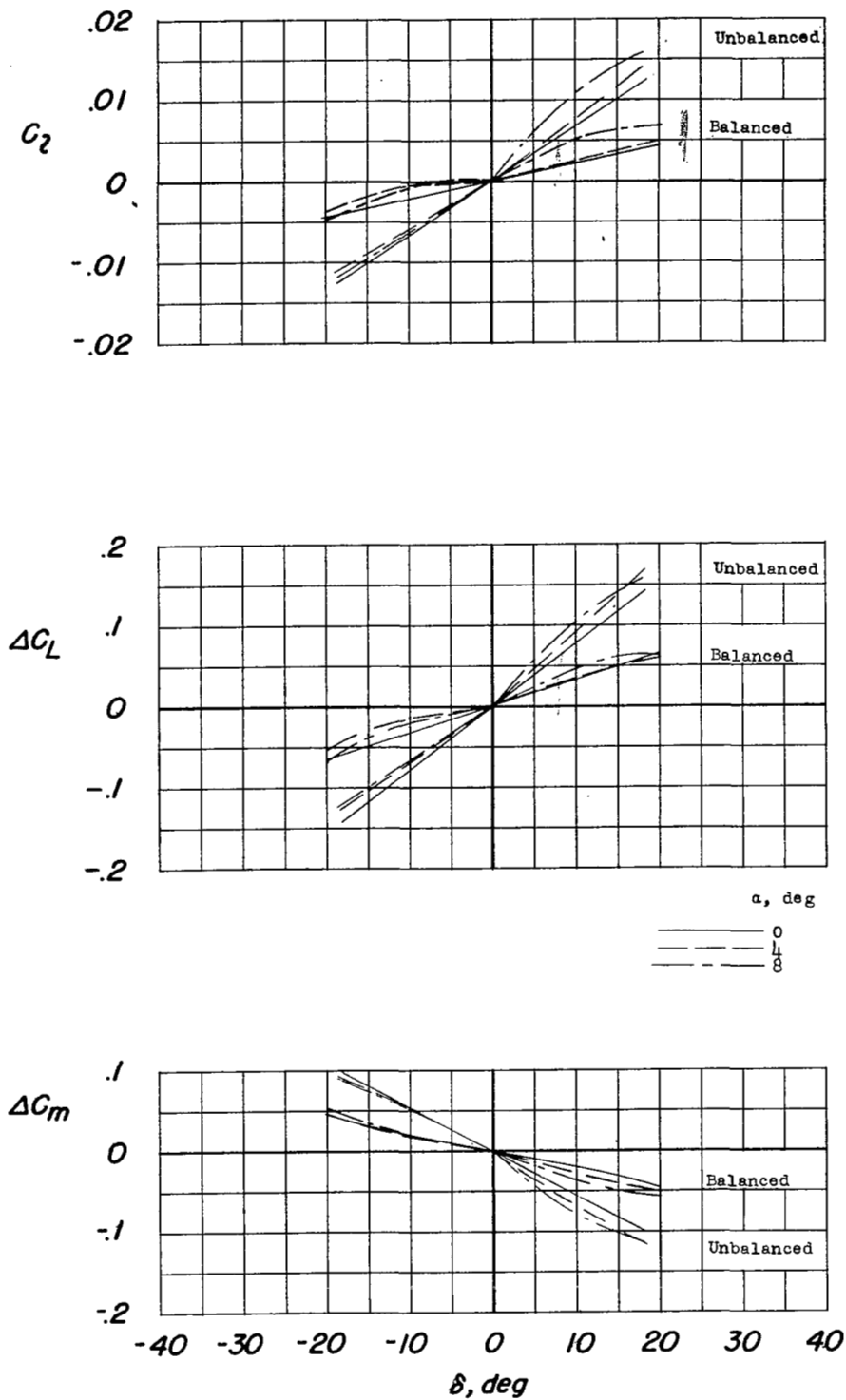
(b) $M = 0.865$.

Figure 8.- Continued.



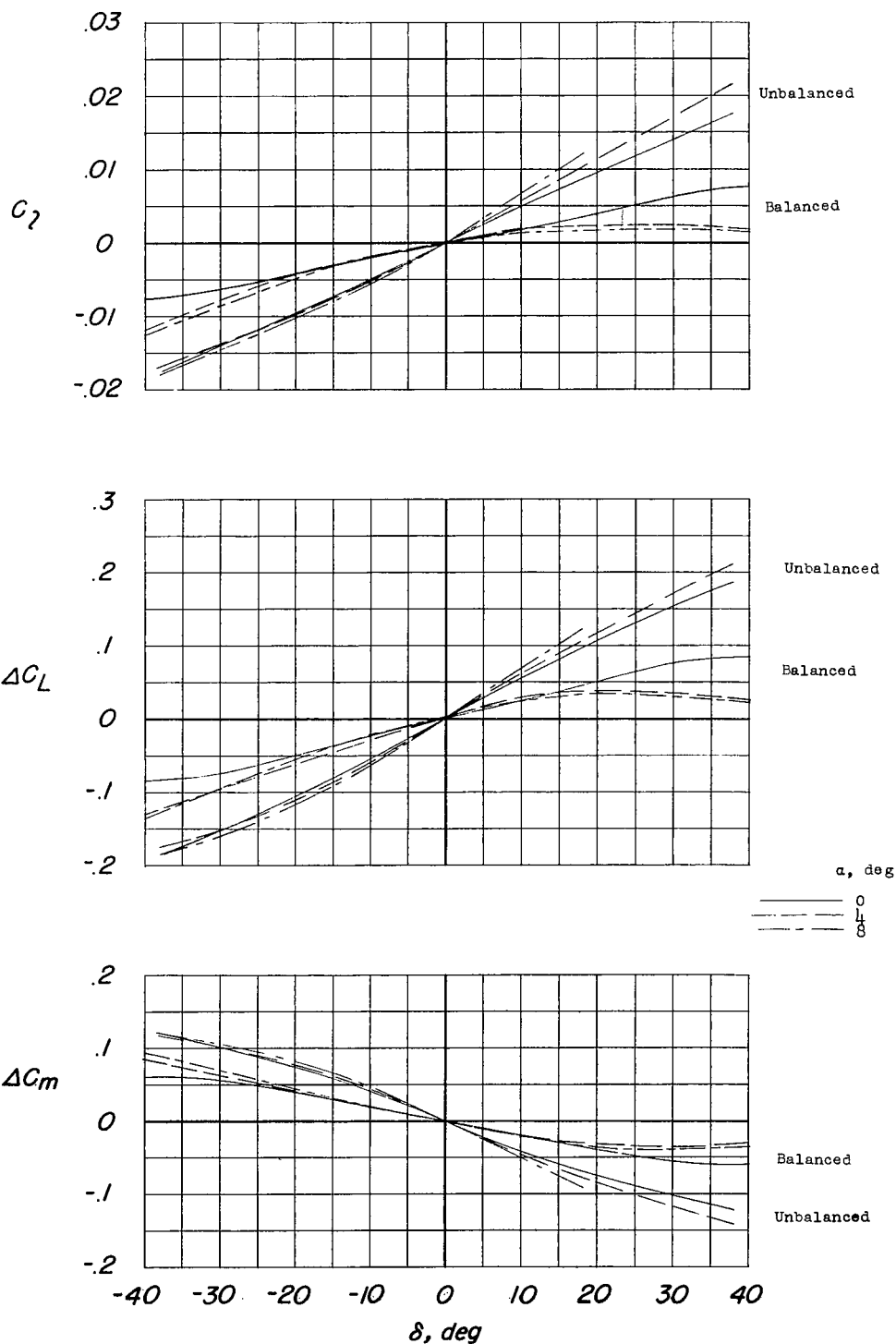
(c) $M = 0.975$.

Figure 8.- Continued.



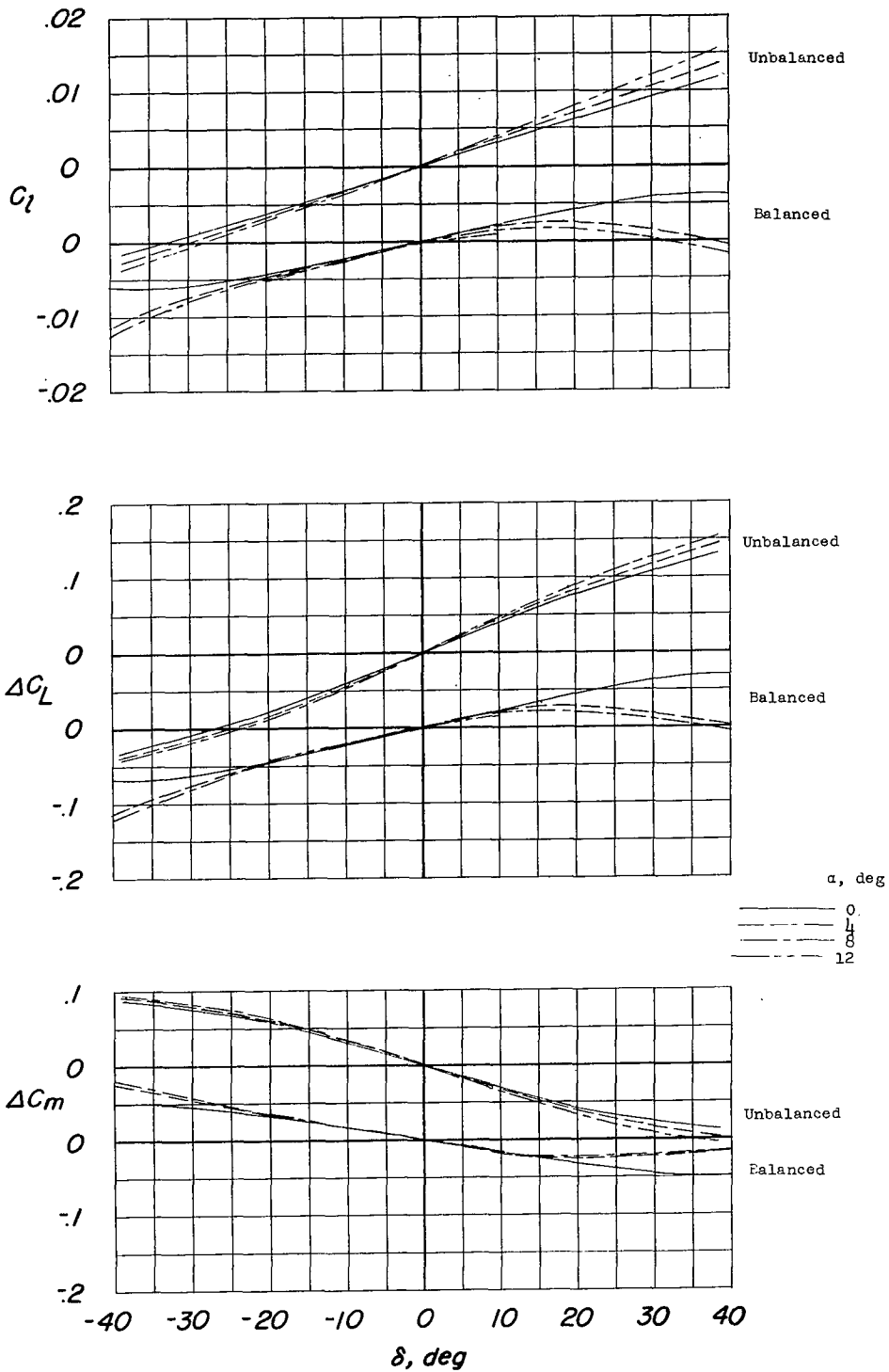
(d) $M = 1.125$.

Figure 8.- Continued.



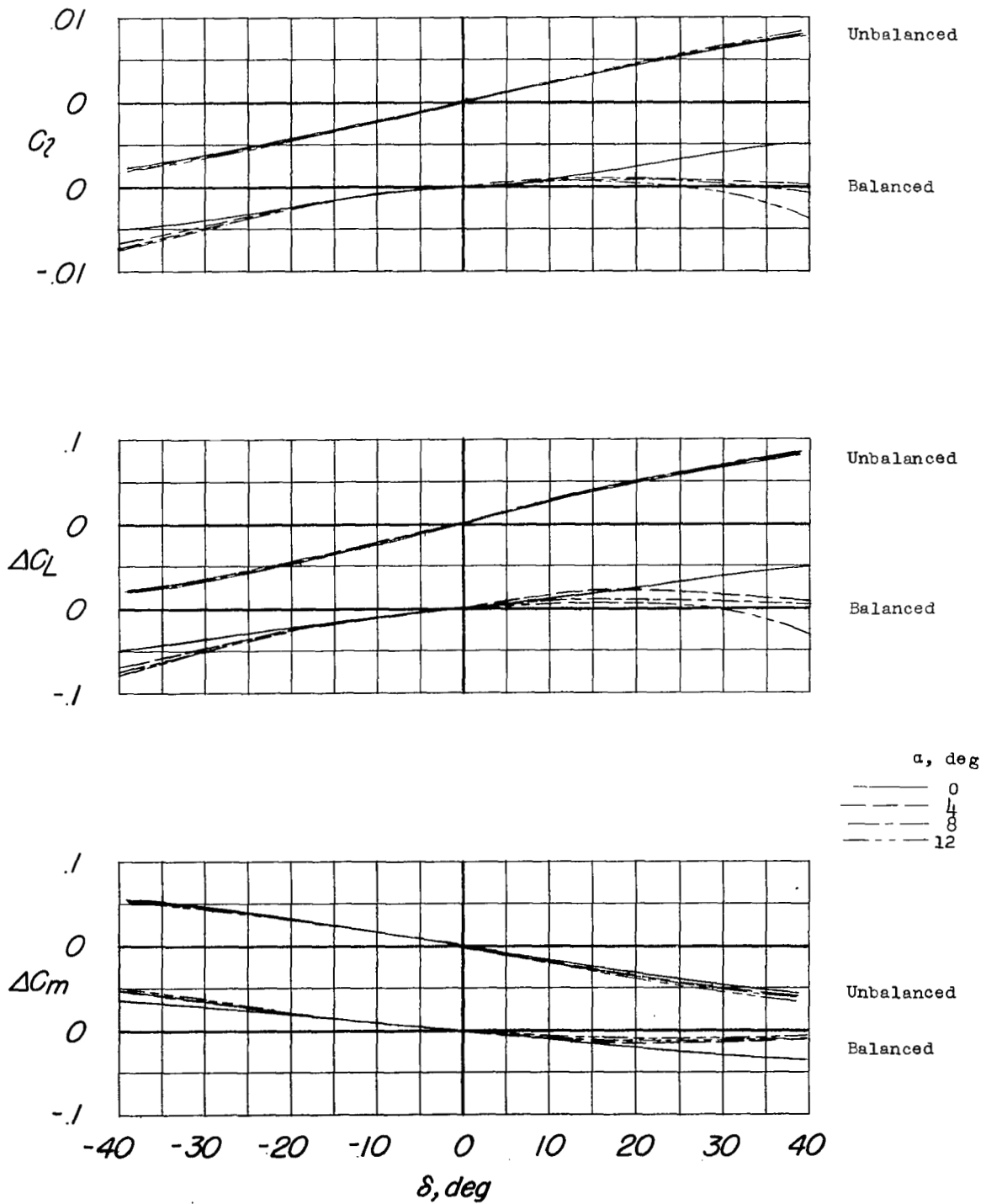
(e) $M = 1.25$.

Figure 8.- Continued.



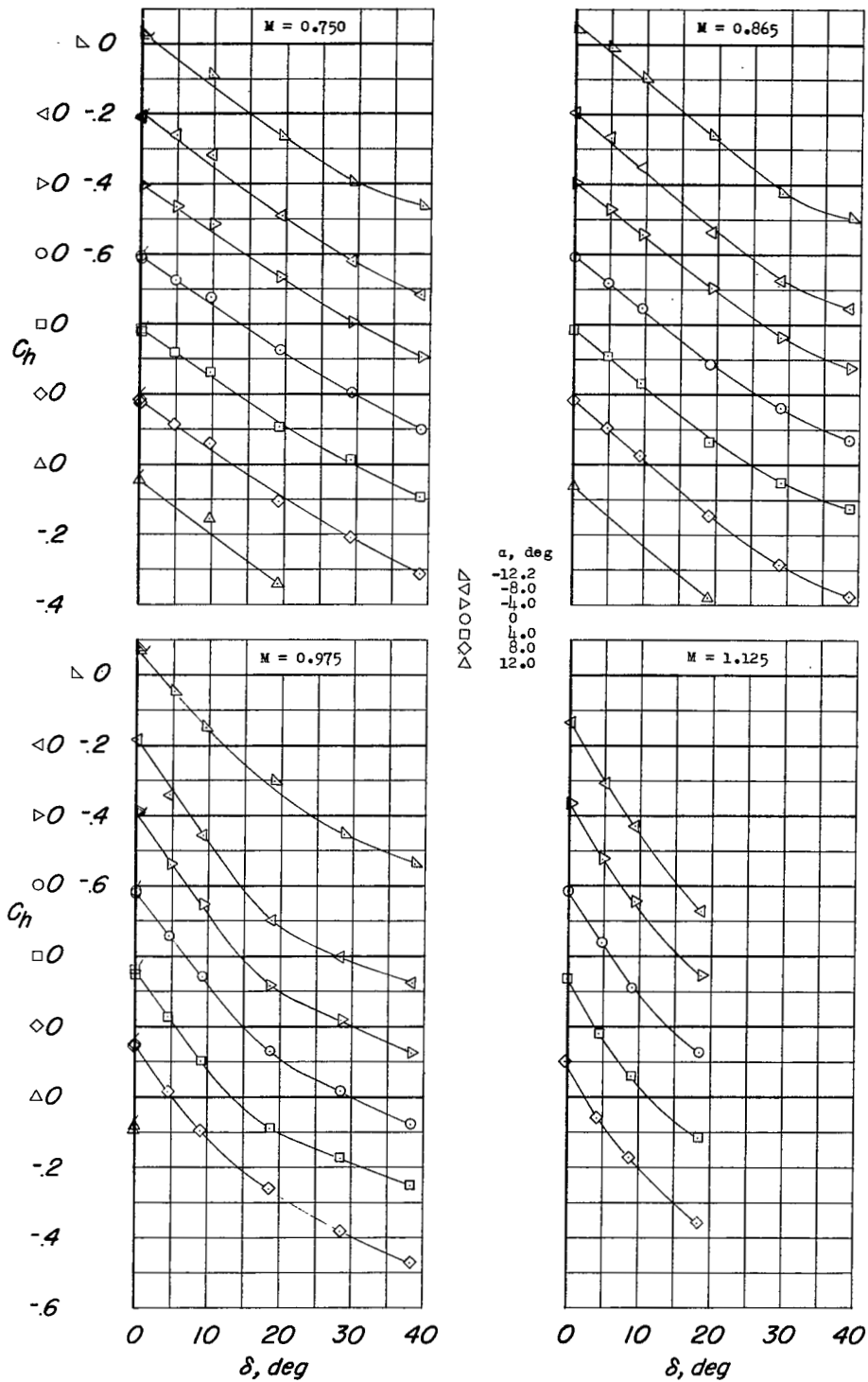
(f) $M = 1.41$.

Figure 8.- Continued.



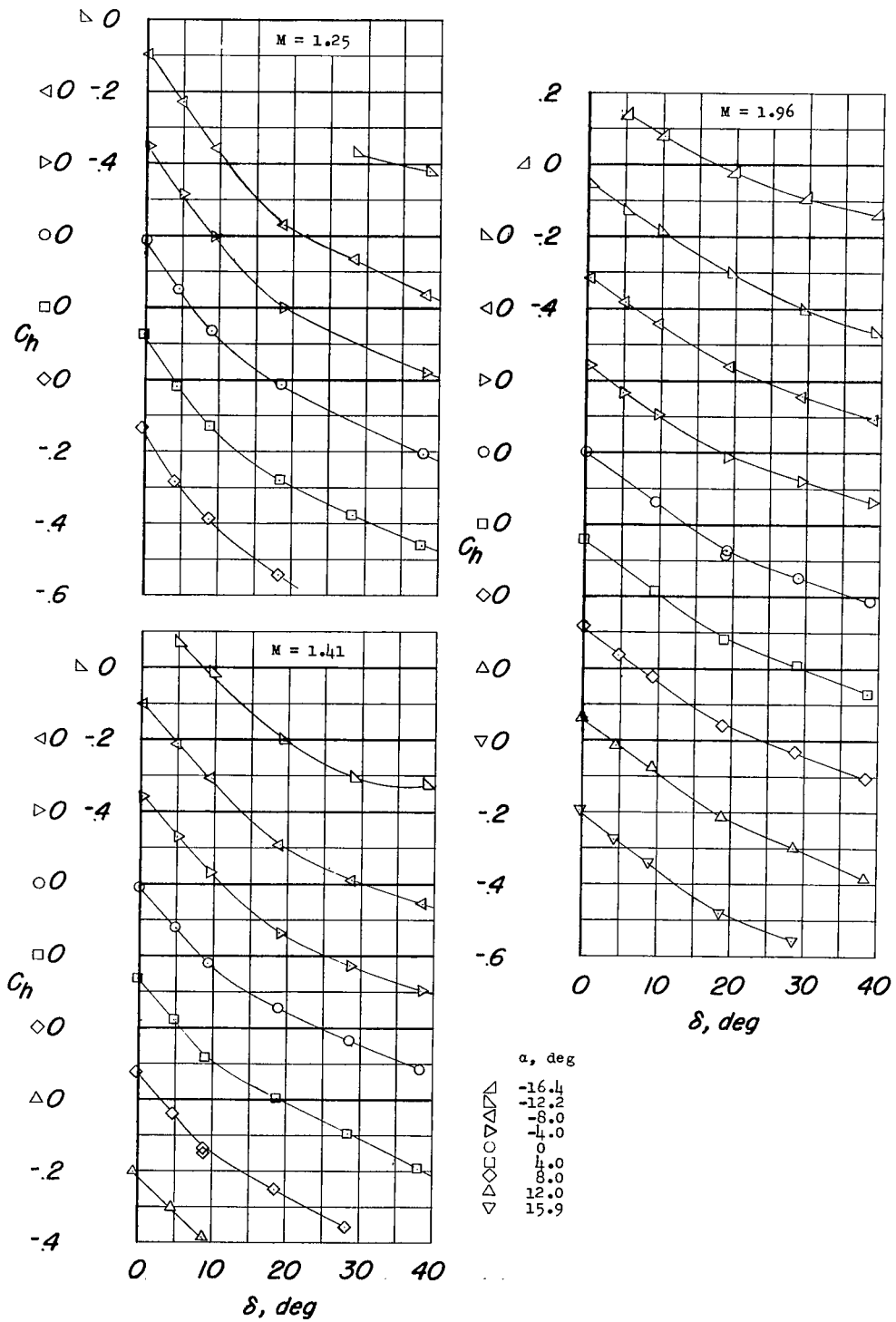
(g) $M = 1.96$.

Figure 8.- Concluded.



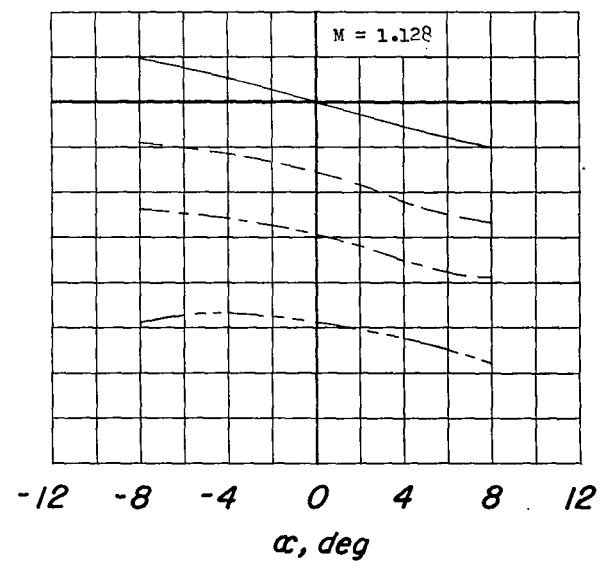
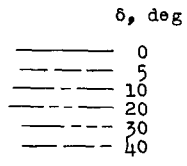
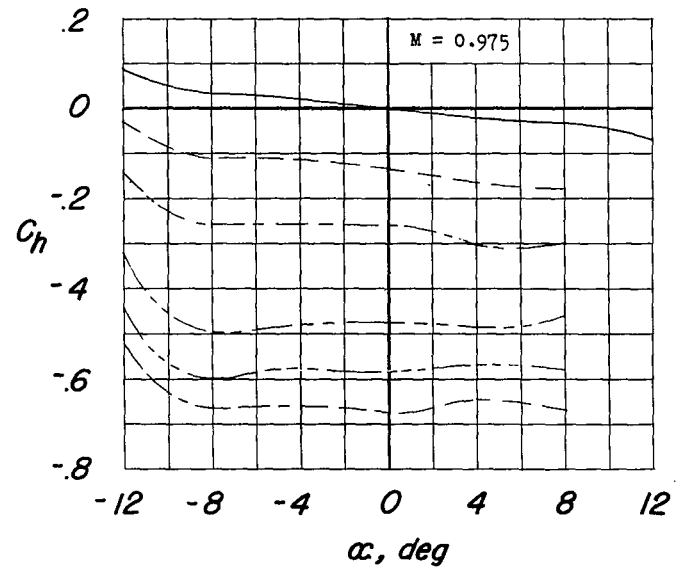
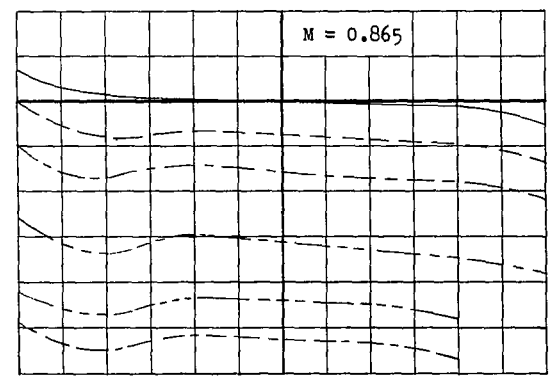
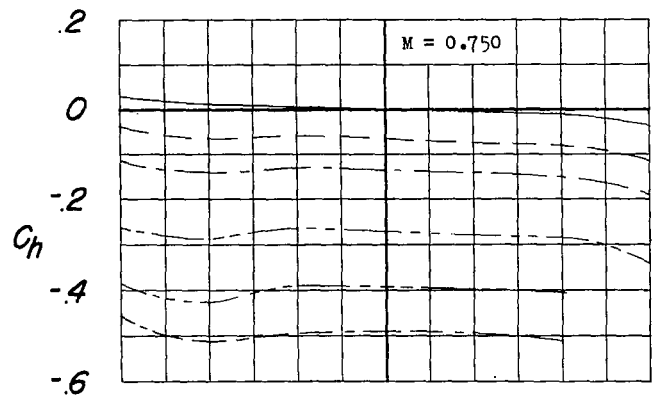
(a) C_h against δ .

Figure 9.- Hinge-moment characteristics of the unbalanced control.



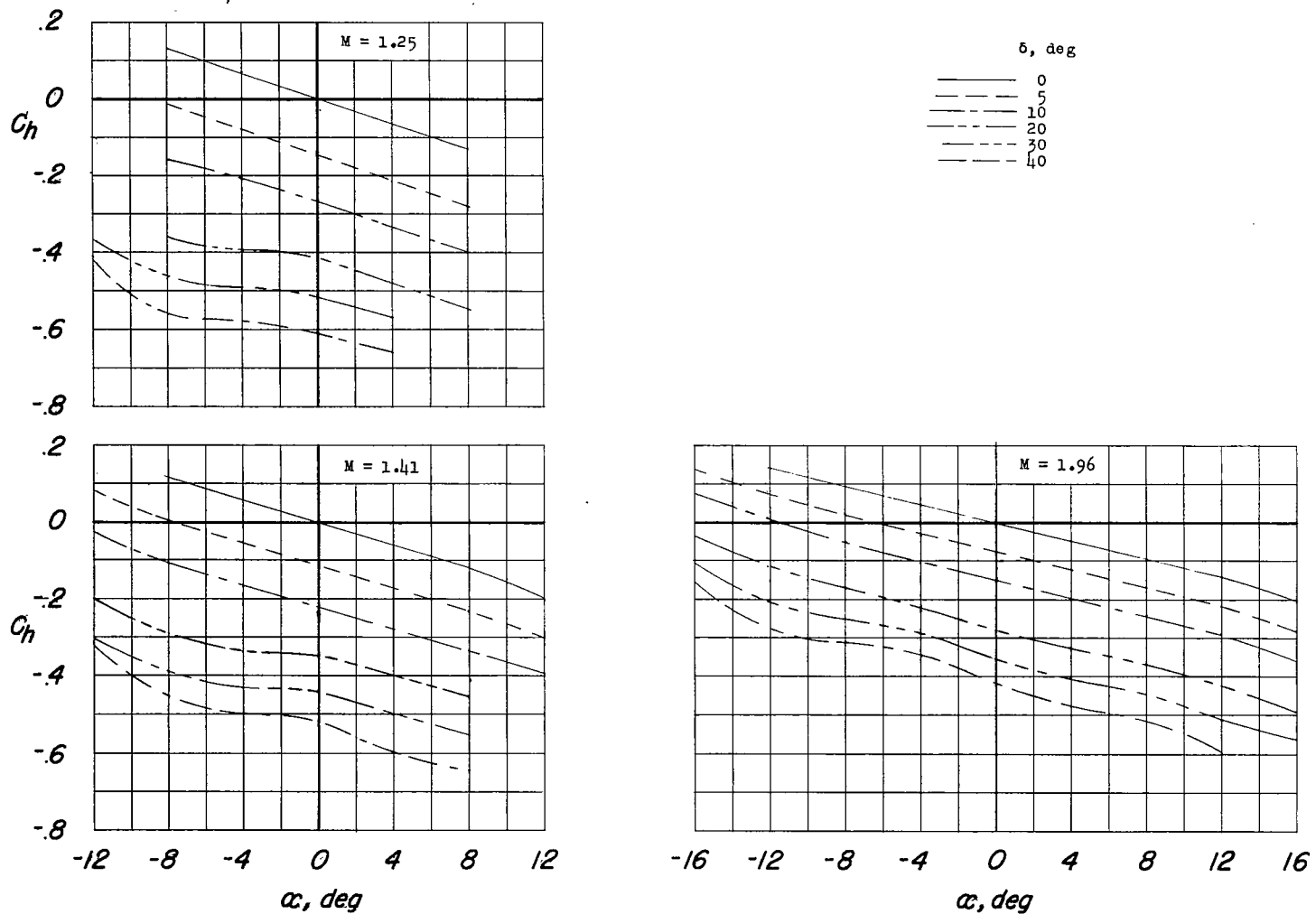
(b) C_h against δ .

Figure 9.- Continued.



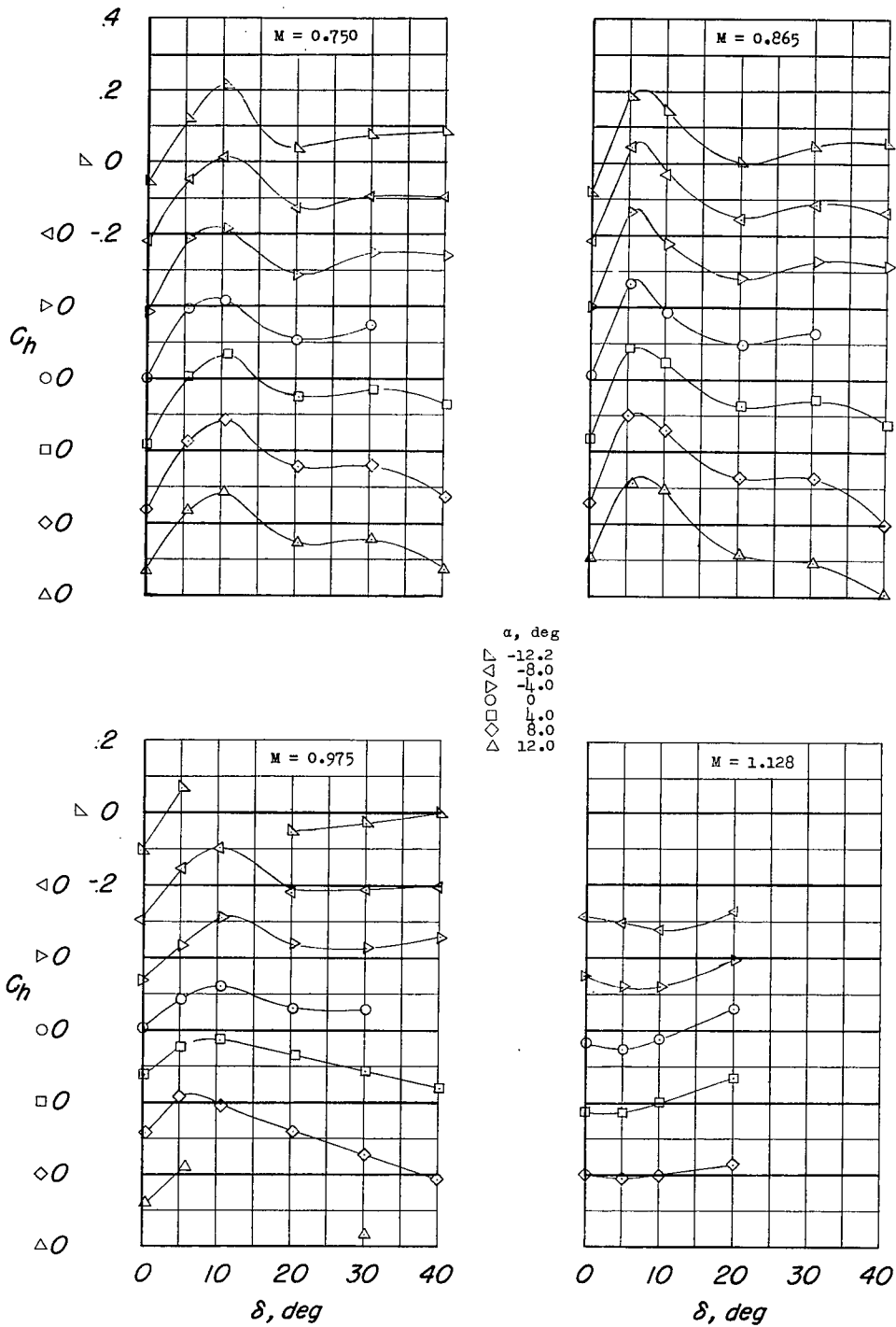
(c) C_h against α .

Figure 9.- Continued.



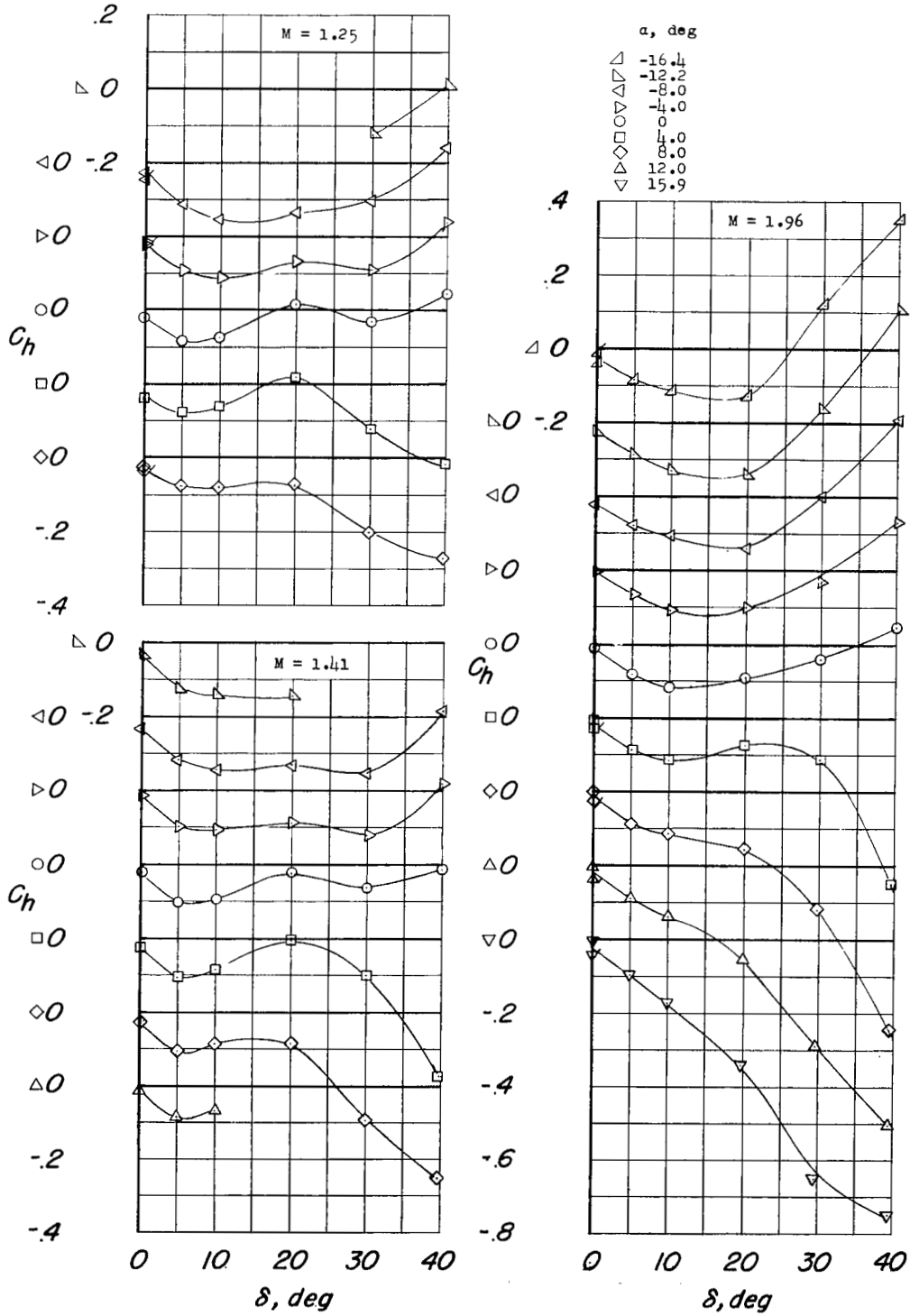
(d) C_h against α .

Figure 9.- Concluded.



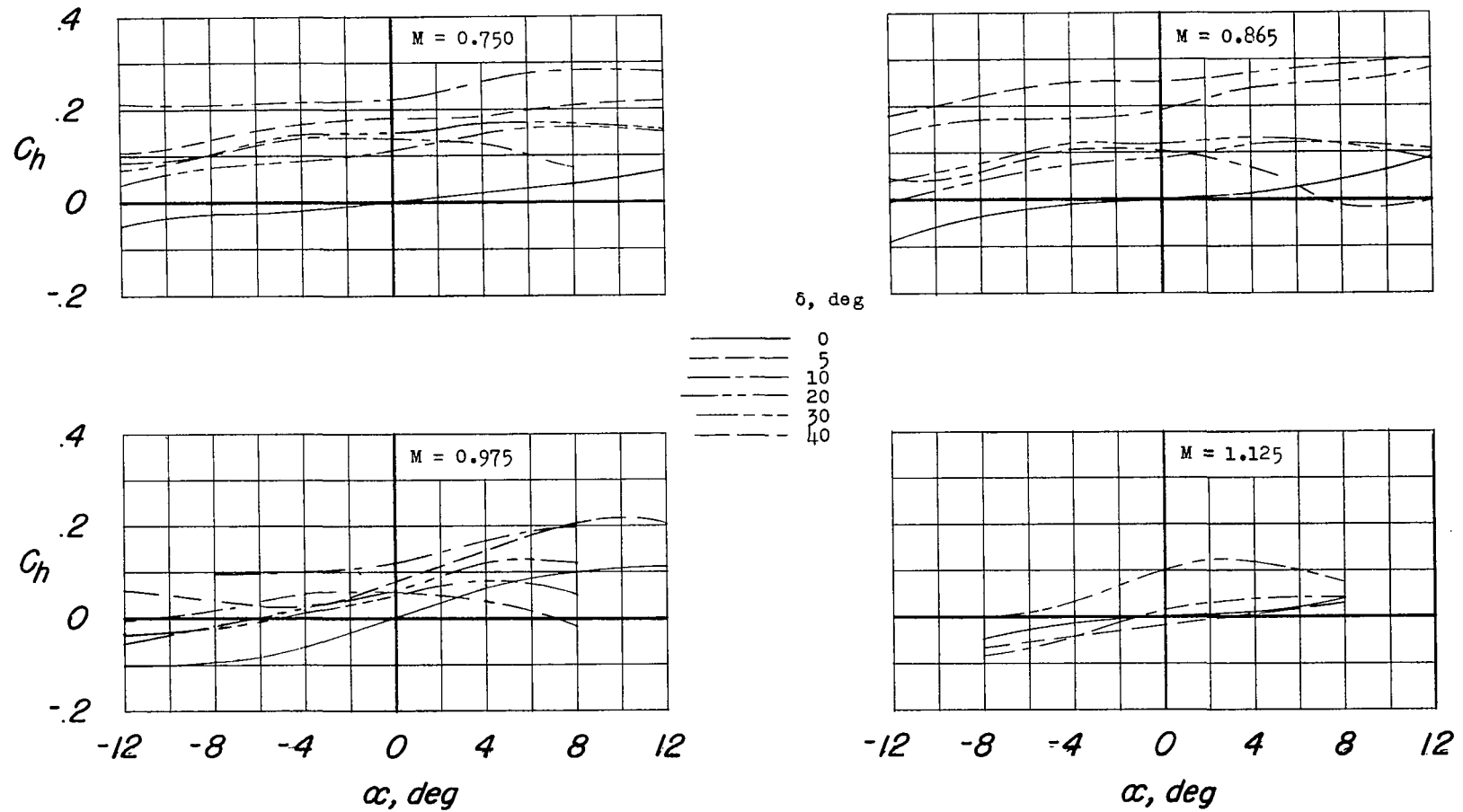
(a) C_h against δ .

Figure 10.- Hinge-moment characteristics of the 100-percent balanced control.



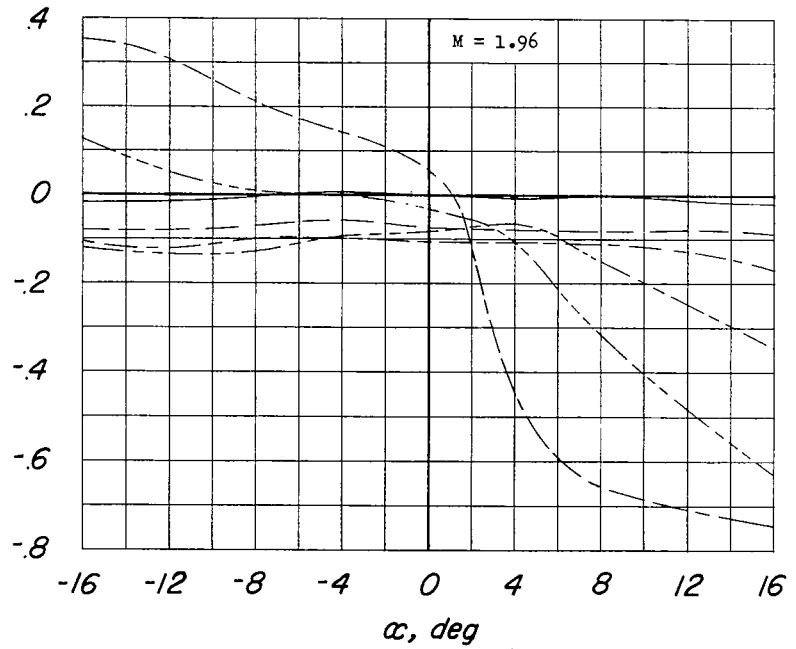
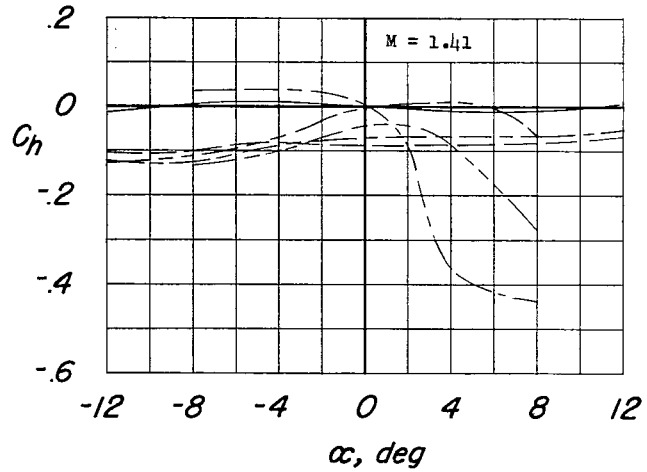
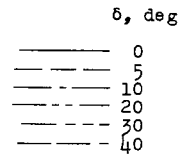
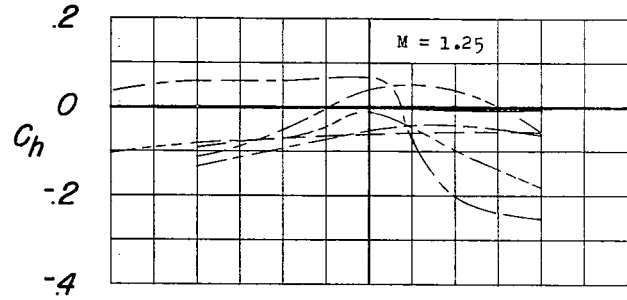
(b) C_h against δ .

Figure 10.- Continued.



(c) C_h against α .

Figure 10.- Continued.



(d) C_h against α .

Figure 10.- Concluded.

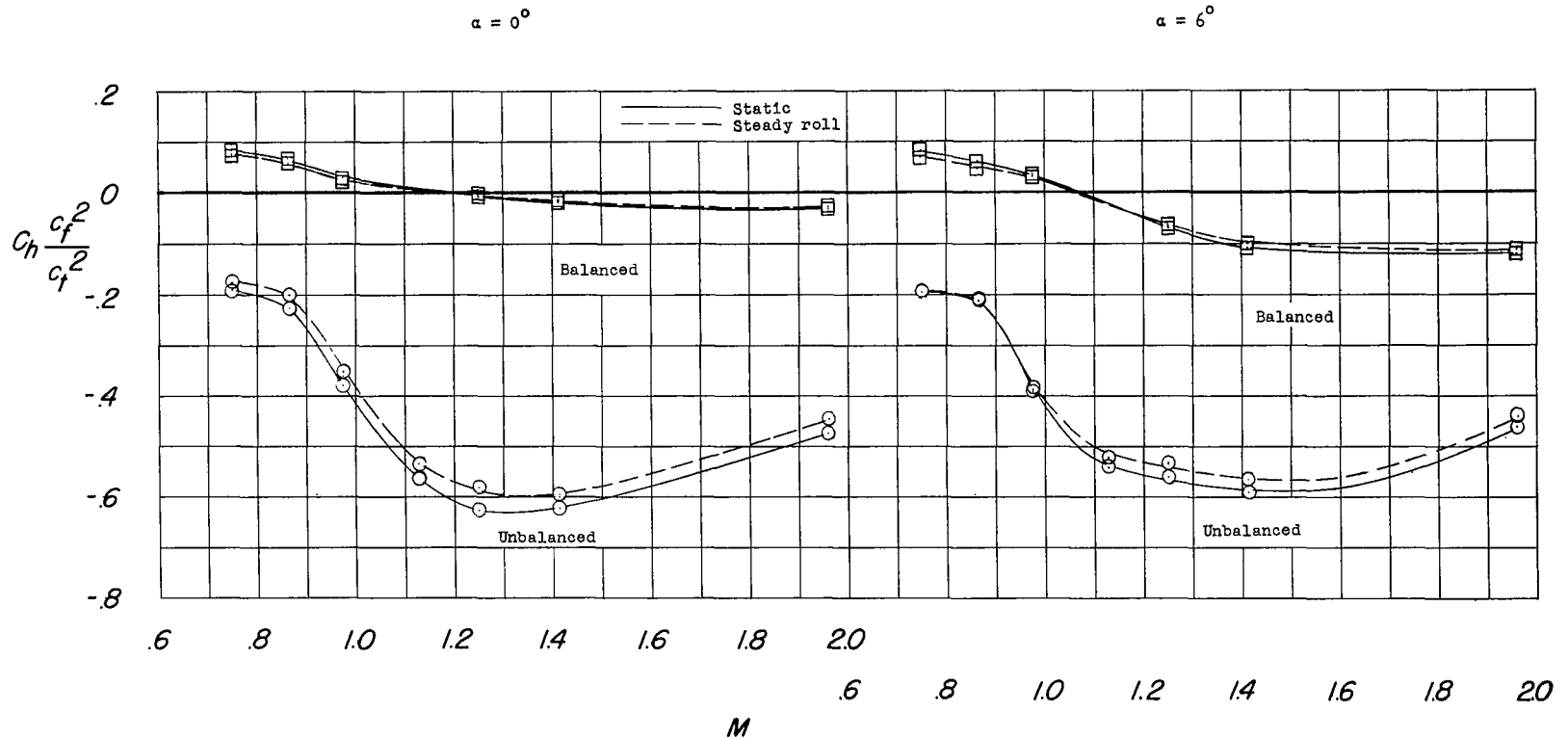


Figure 11.- Comparison of the variation with Mach number of the hinge-moment parameter $C_h \frac{c_f^2}{c_t^2}$ for the balanced and unbalanced controls; comparison is made at rolling moments required for 3.5 radians per second roll rates of wings having 660 square feet of area and operating at 40,000 feet.

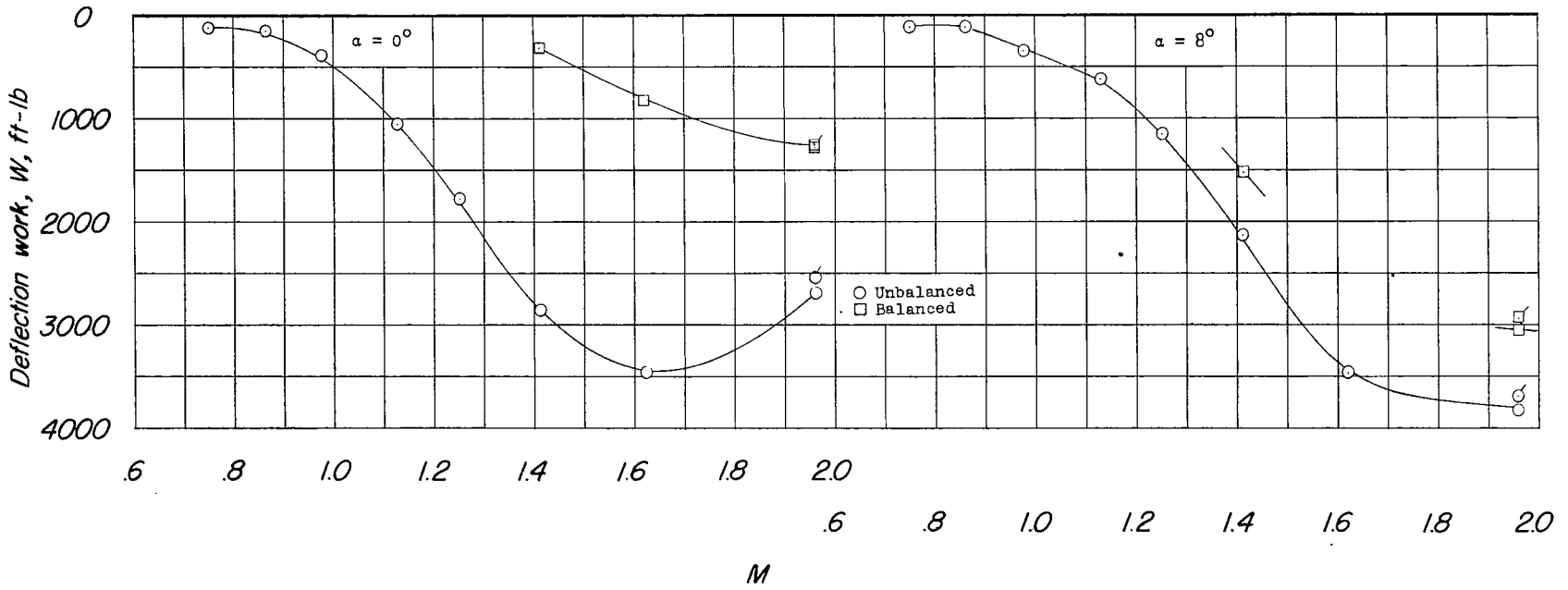


Figure 12.- Comparison of deflection work of two controls producing rolling moments required for 3.5 radians per second roll rates of wings having 660 square feet of area and operating at 40,000 feet. Unflagged symbols denote static case; flagged symbols denote rolling case.

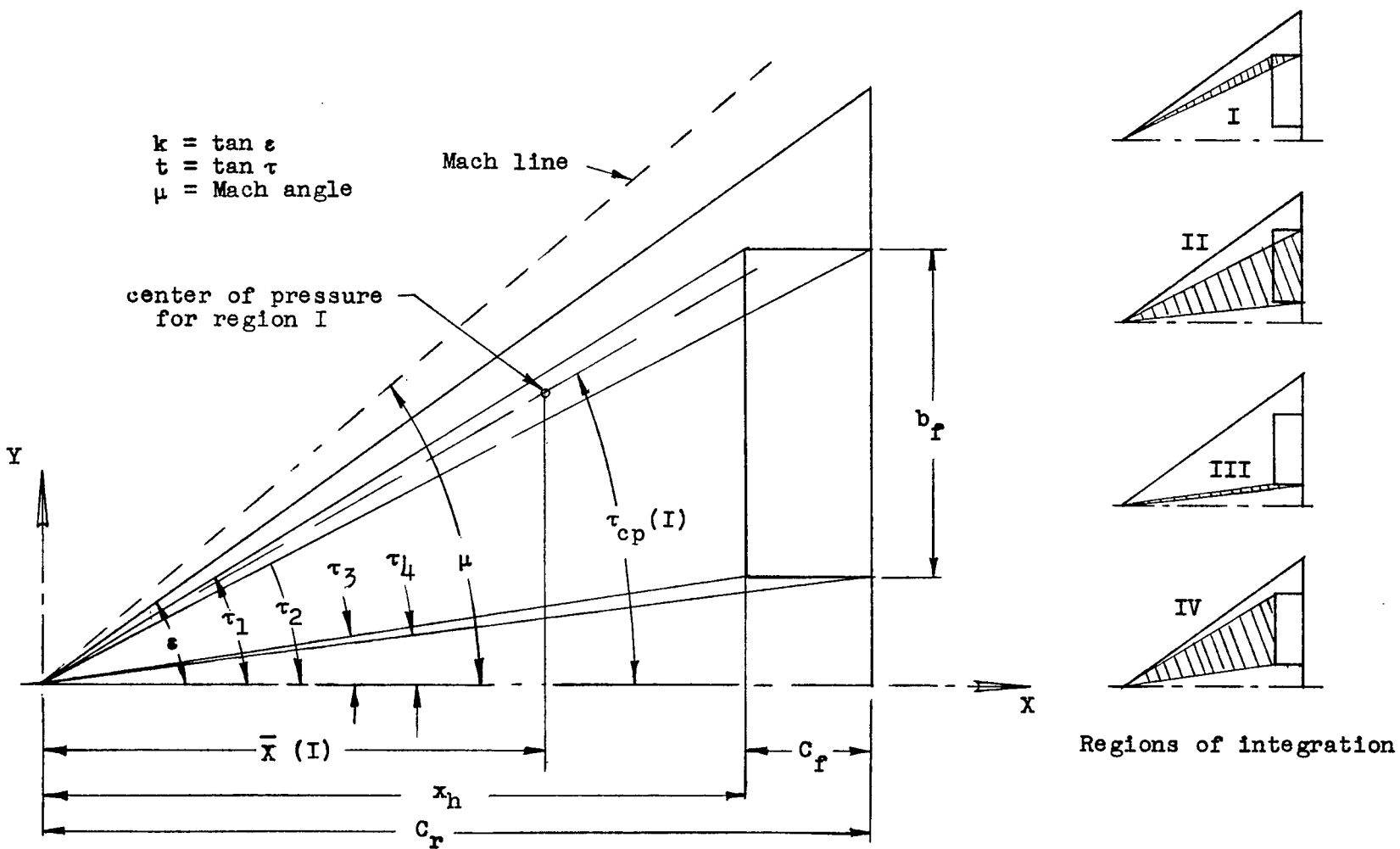
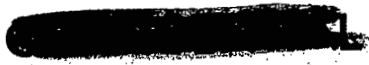


Figure 13.- Sketch of right wing panel of delta wing and trailing-edge flap showing regions of integration for determination of $C_{n\alpha}$.



NASA Technical Library



3 1176 01437 1653

